Transport and Energetic Particle Confinement Issues for Compact Stellarators

D.A. Spong

Oak Ridge National Laboratory, P.O. Box 2009, Oak Ridge, TN 37831-8073

in collaboration with Steve Hirshman, Jim Lyon, Lee Berry, Dave Mikkelsen

US/Japan JIFT Workshop on "Theoretical Considerations on Helical Plasmas".
November 18 - 20, 2002
Princeton Plasma Physics Lab.

QPS is a very low aspect ratio (A = 2.7) Quasi-poloidal stellarator

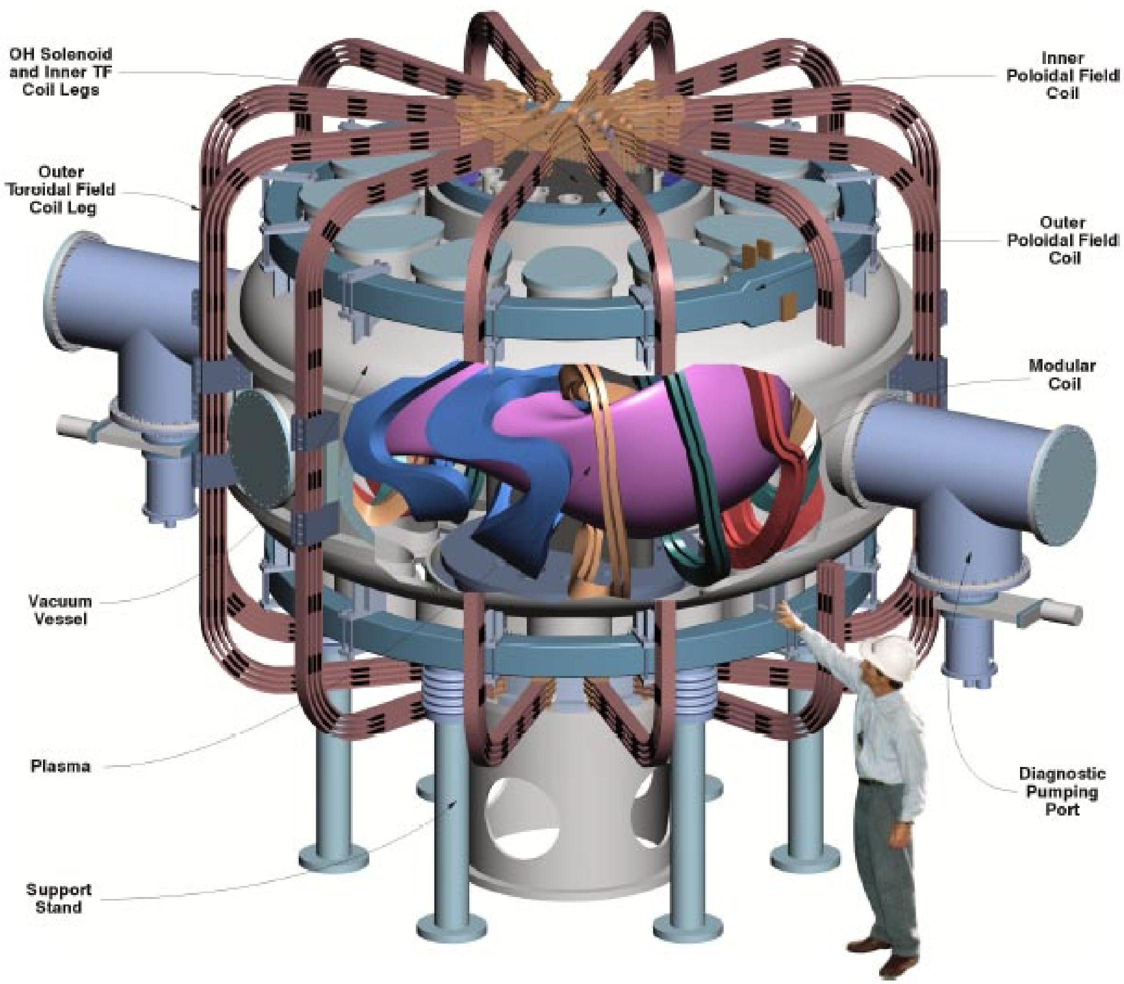

- $\langle R_0 \rangle = 0.9$ m, $\langle a \rangle = 0.33$ m, $\langle B \rangle = 1$ T $\pm$ 0.2T for 1sec, $I_p \leq 150$ kA, $P_{ECH} = 0.6$-1.2 Mw, $P_{ICH} = 1$-3 Mw
- This experiment will test:
  - Equilibrium robustness
  - Neoclassical and anomalous transport
    - Near conservation of P_θ implies banana width involves toroidal field rather than poloidal field
  - Stability limits up to $\langle\beta\rangle = 2.5\%$
  - Bootstrap current effects
  - Reduced poloidal viscosity effects on shear flow transport reduction
  - Configurational flexibility

Our transport analysis has focused on optimization targets and comparisons between configurations

Optimization Strategy

- QOS optimizations (1996 - 1999)
  - J^*, J, B_{min}, B_{max}
  - DKES
- QPS optimizations (2000 - present)
  - ε_{eff}
  - Poloidal symmetry
  - DKES

Evaluation Tools

- NEO ε_{eff}, Poloidal symmetry
- DKES
  - Setup, mode selection
  - Parallel runs
  - Energy integration
- DELTA5D Monte Carlo
  - Global full-f model
  - ICRF heating
  - NBI heating efficiency
  - Alpha losses
  - Bootstrap current
- 1-1/2 D model

However, with the QPS configuration becoming fixed, we are shifting over to flexibility studies and transport predictions.

NEO code provides $\varepsilon_{eff}^{3/2} \sim D^{1/\nu}, \chi^{1/\nu}$. Comparison of different configurations:

NEO ε_{eff} code

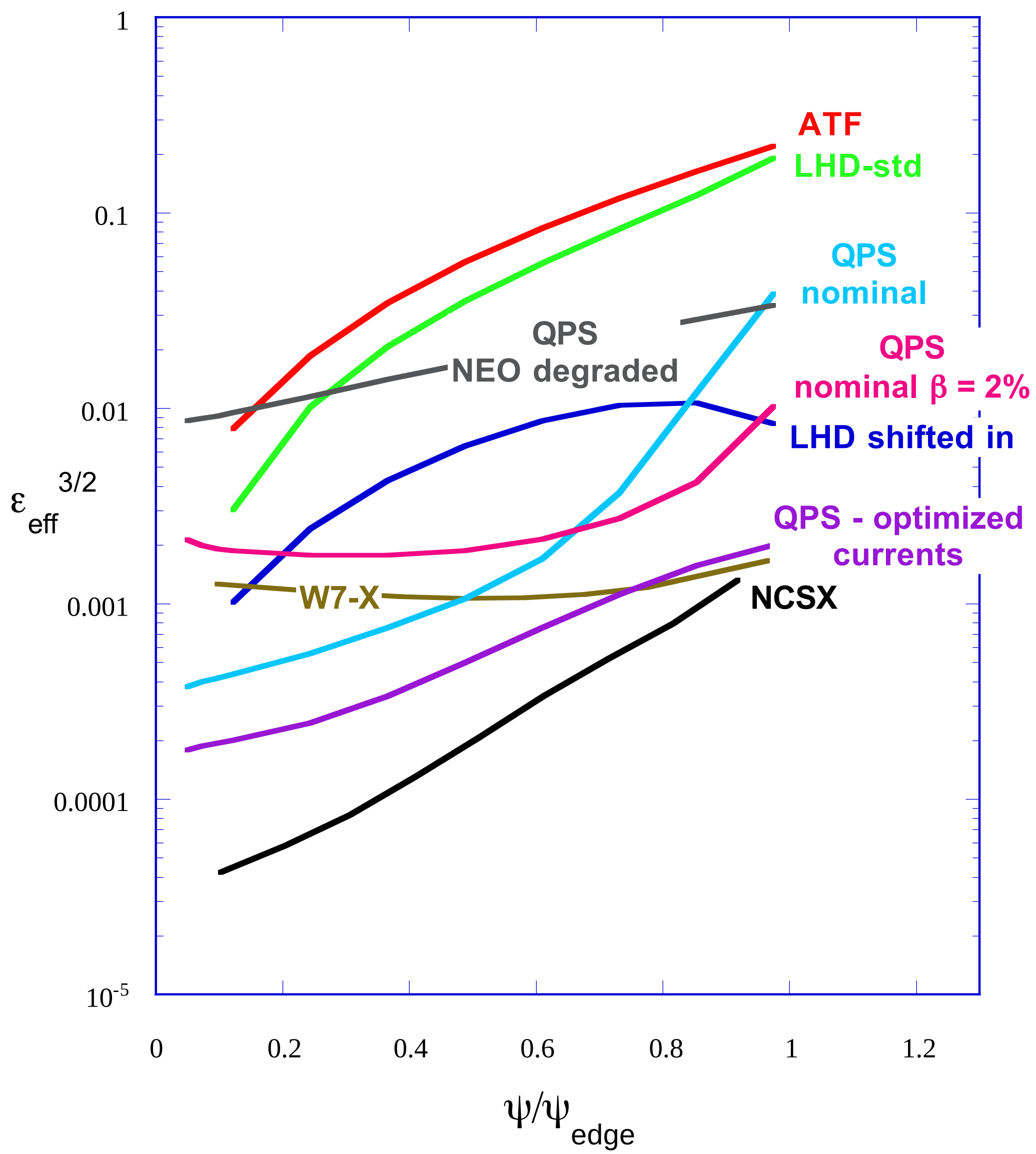

DKES transport dependencies show that both $L_{11} \propto \nu^{1/2}$ and $L_{11} \propto 1/\nu$ regimes are accessed.

These ranges are based on the maximum n, T in the profile, $e\phi/kT(a) = 1$, and looking from thermal energy to 9 times thermal (as sampled by velocity integrals for χ)

- **ECH electrons**:
  - $7\times10^{-5} < \nu/v < 10^{-3}$
  - $8\times10^{-5} < E/v < 2\times10^{-4}$
- **ECH ions**:
  - $6\times10^{-3} < \nu/v < 7\times10^{-2}$
  - $10^{-2} < E/v < 3\times10^{-2}$
- **ICH electrons:**
  - $3\times10^{-3} < \nu/v < 4\times10^{-2}$
  - $5\times10^{-5} < E/v < 2\times10^{-4}$
- **ICH ions:**
  - $2\times10^{-3} < \nu/v < 3\times10^{-2}$
  - $2\times10^{-3} < E/v < 6\times10^{-3}$

Note: these L11's are based on the gb4 device.

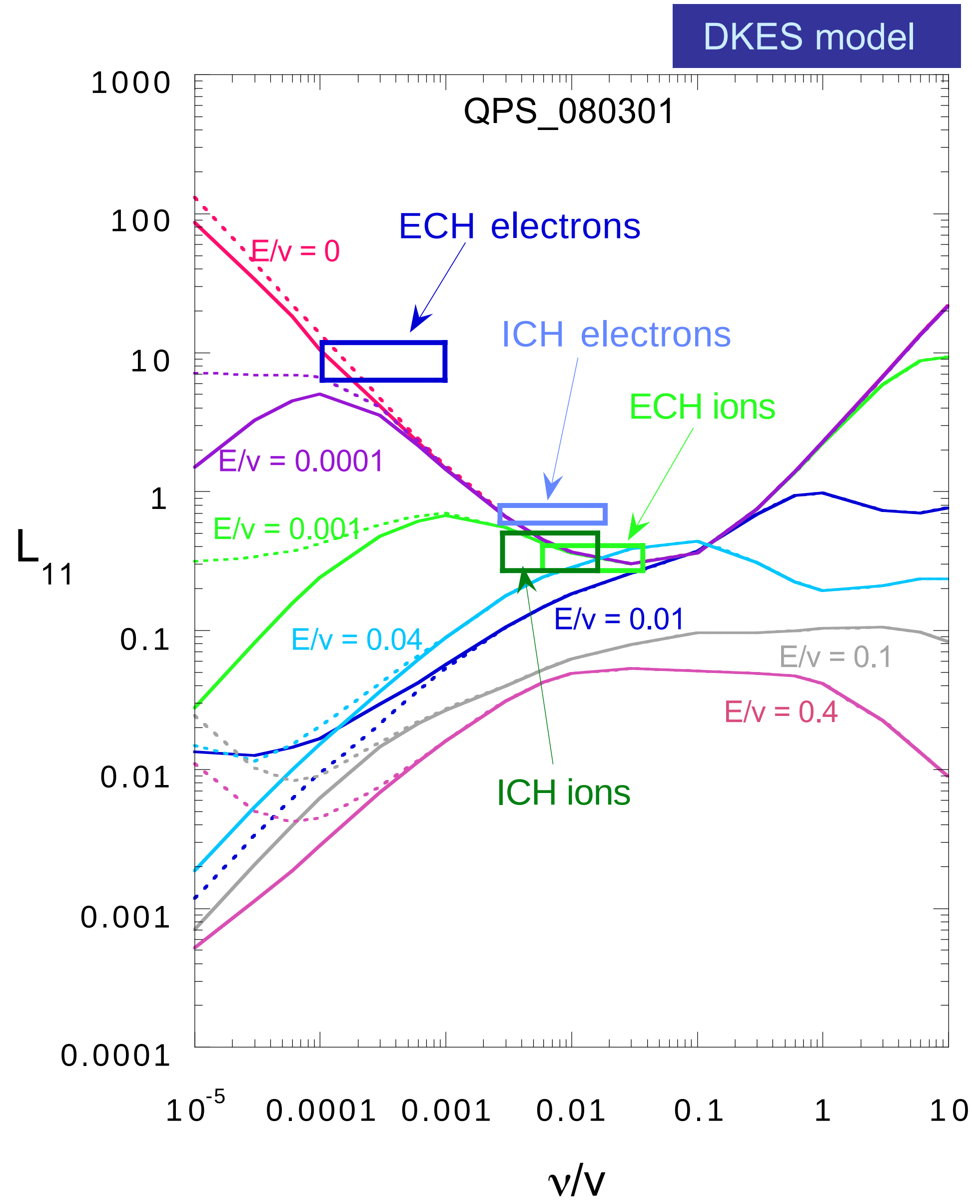

DKES L_{11} transport coefficient at $E_r/v = 0$ and global Monte Carlo lifetimes show similar trends at low collisionality among QPS devices as NEO $\varepsilon_{eff}^{3/2}$ coefficient

DKES/DELTA5D model

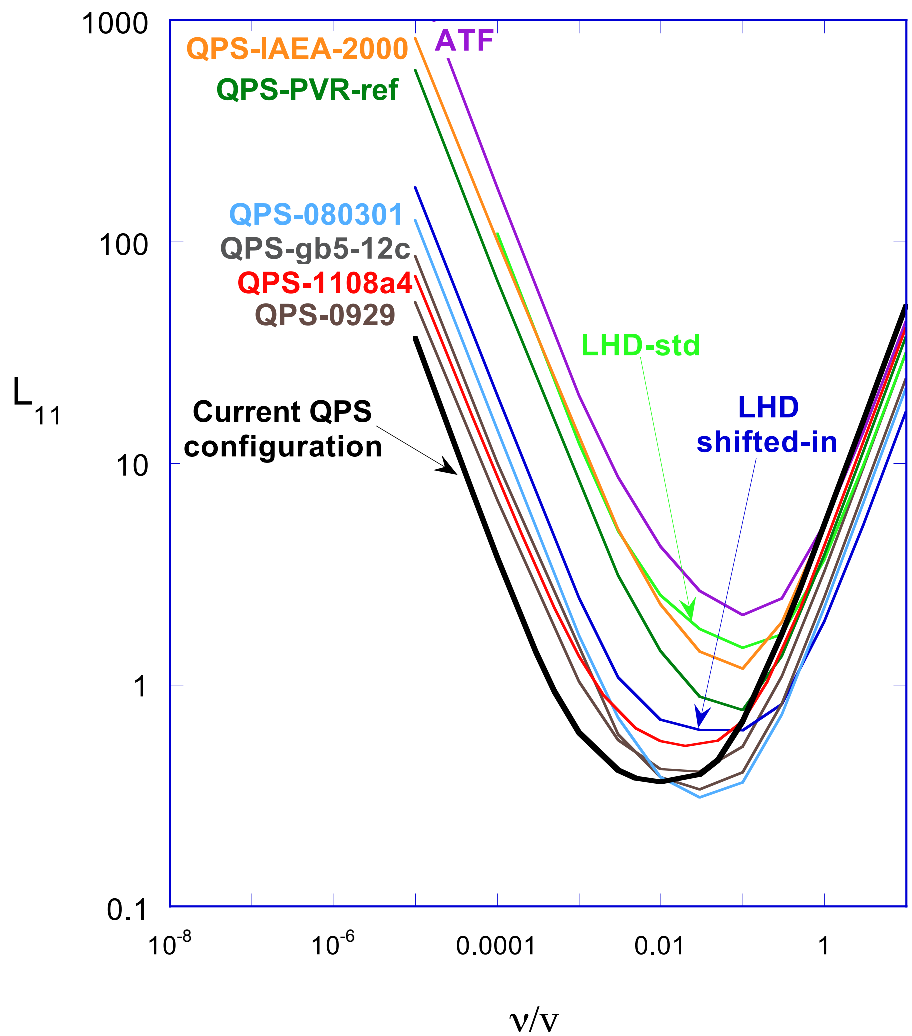

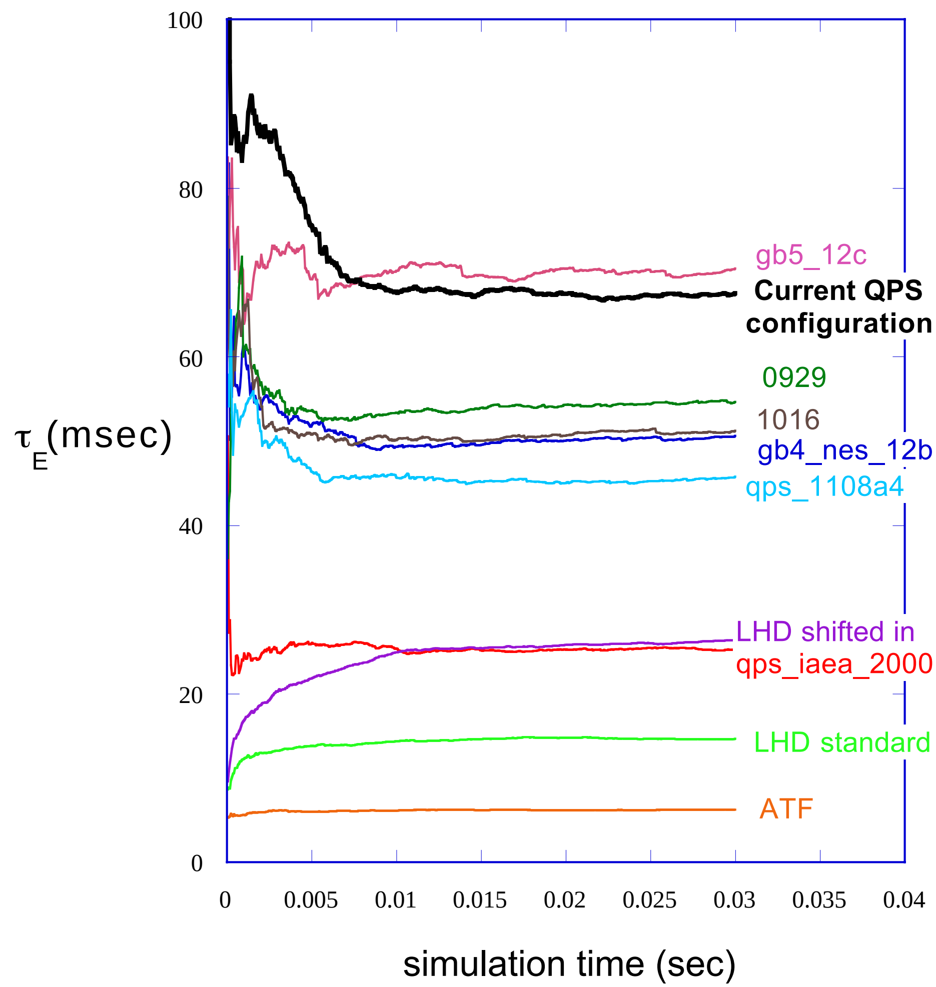

QPS Flexibility Studies

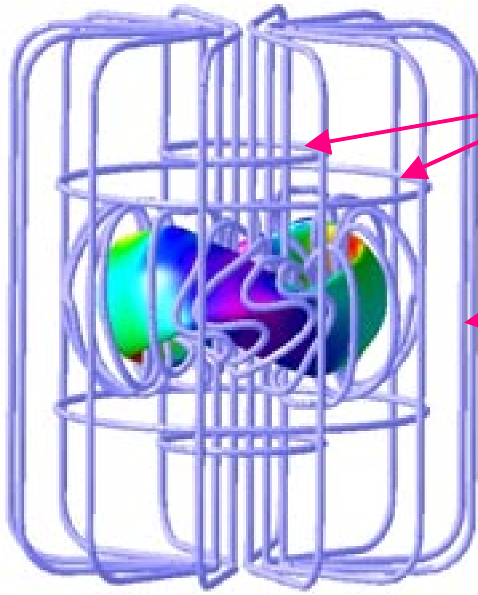

2 vertical field coils

Toroidal 1/R field

4 independently powered modular coils

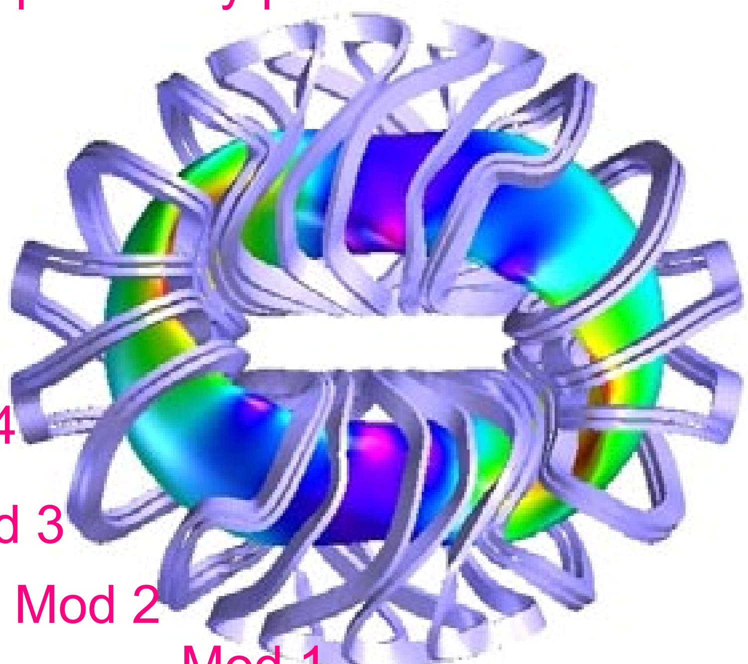

Mod 4

Mod 3

Mod 2

Mod 1 (split coil)

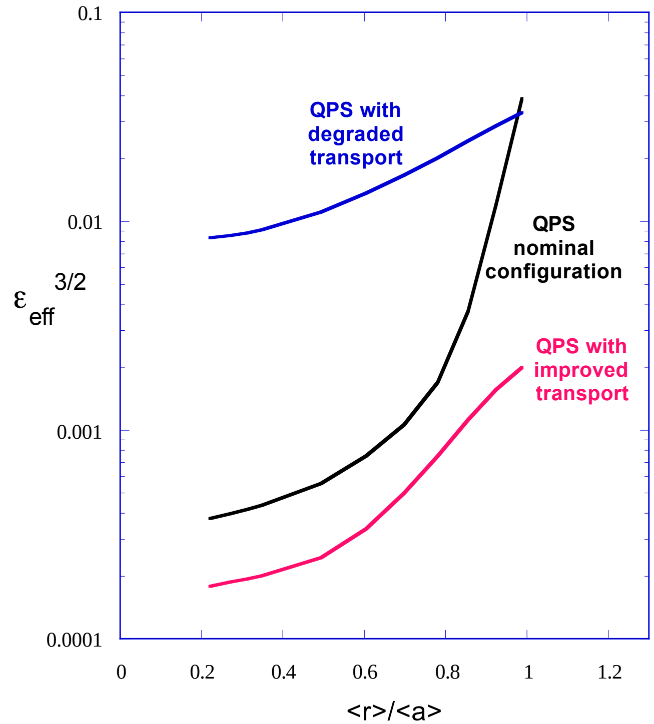

Coil Current distributions

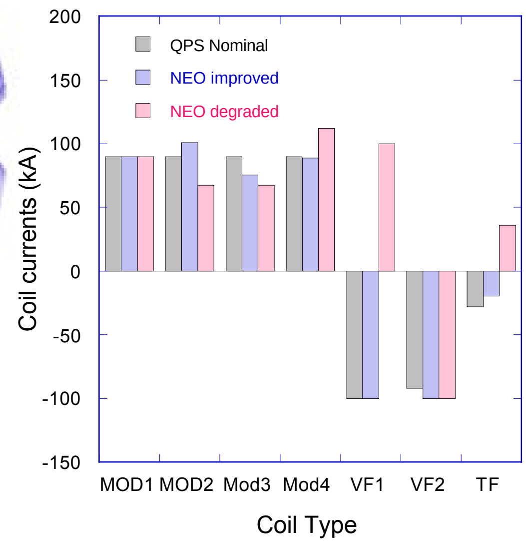

- Modular coil currents can vary ±25%
- Vertical field currents can vary ±100 kA
- Toroidal field currents can vary ±70 kA

QPS Flexibility Studies - effect on |B|

Degraded transport | Nominal configuration | Improved transport

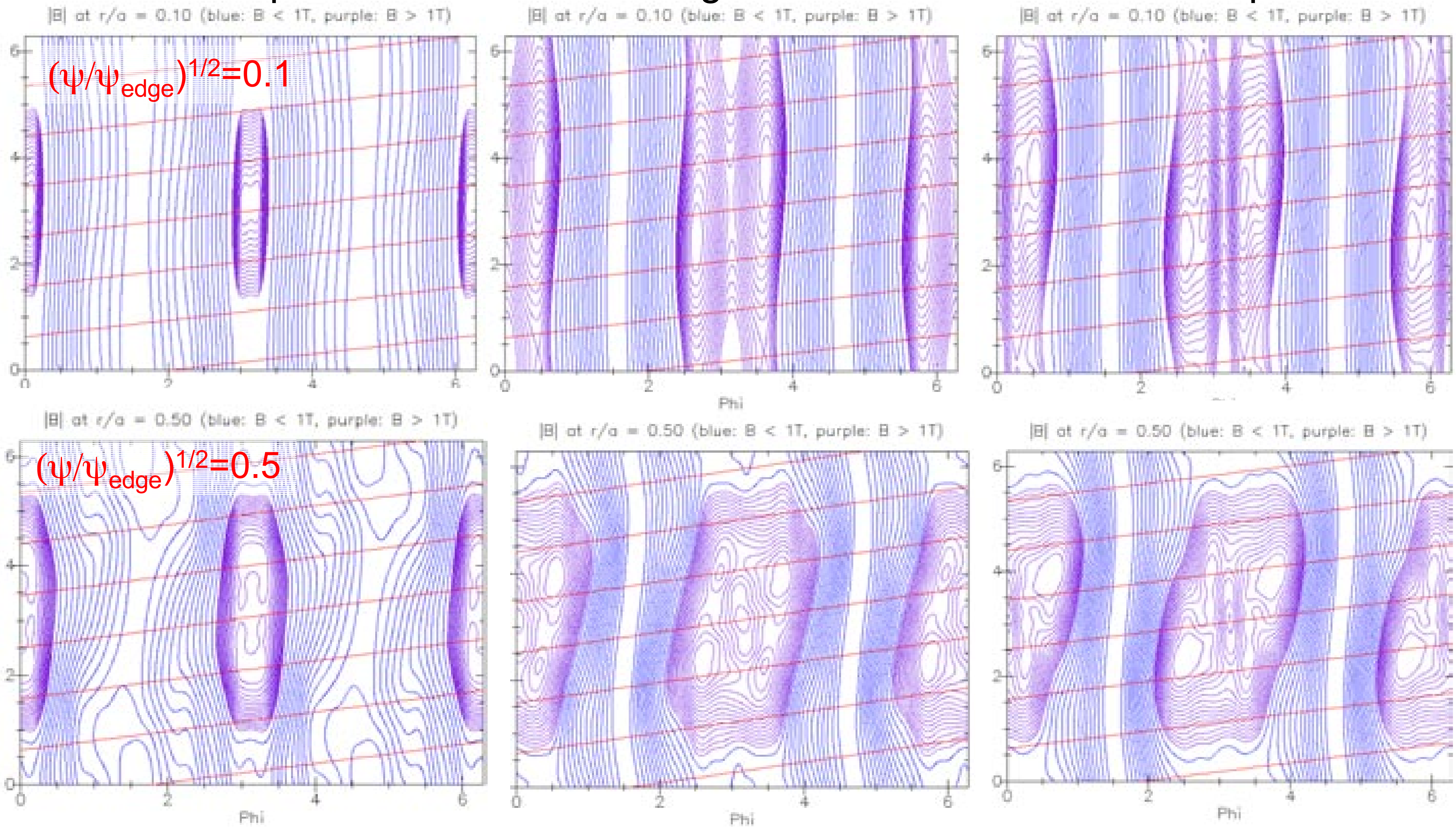

DKES L_{11} coefficient demonstrates sensitivity of transport to coil current optimization

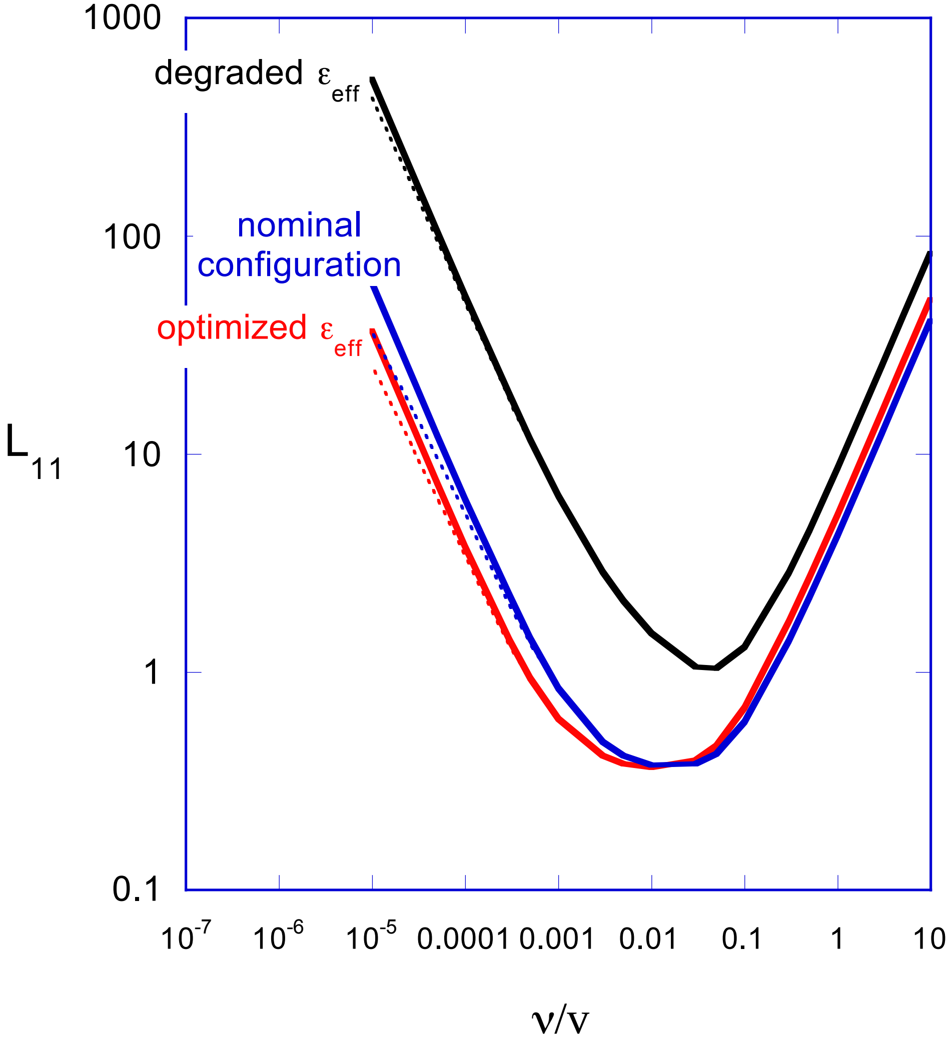

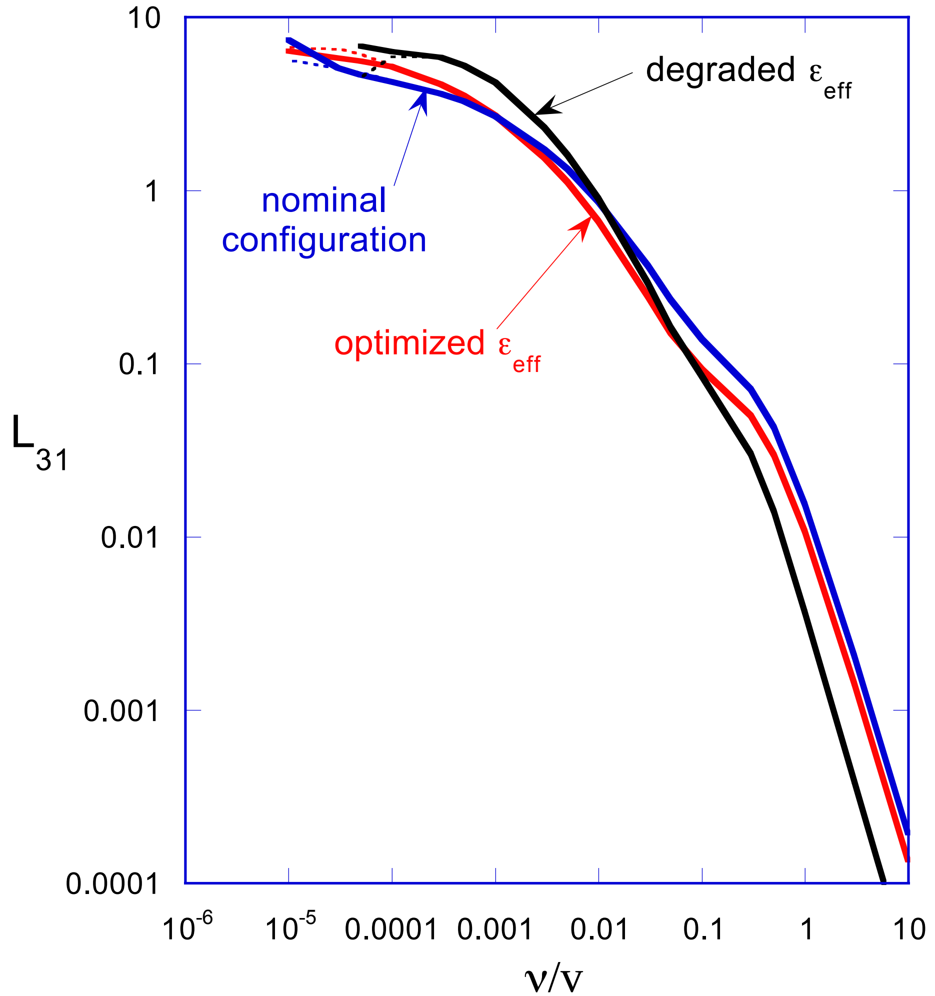

DKES L_{31} coefficient (bootstrap current for recent QPS device (411)

DKES results

(error bars indicate upper/lower bounds)

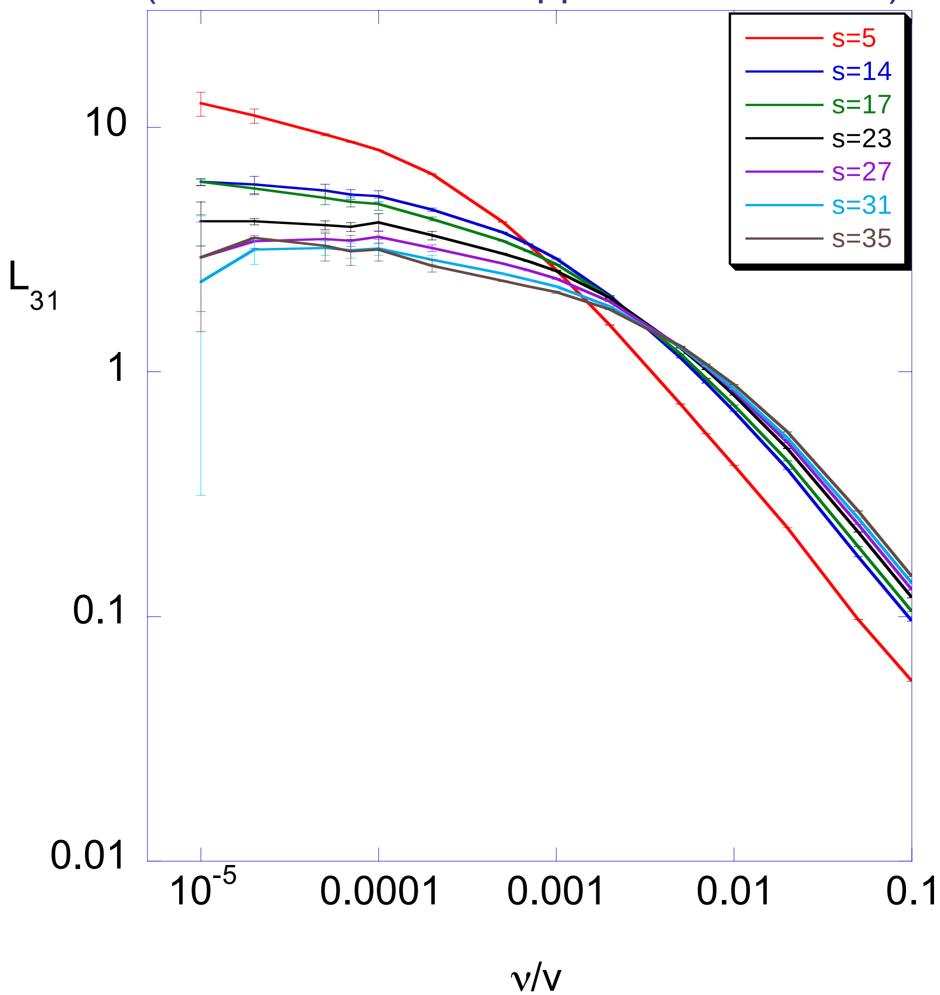

Fits using Padé approximant

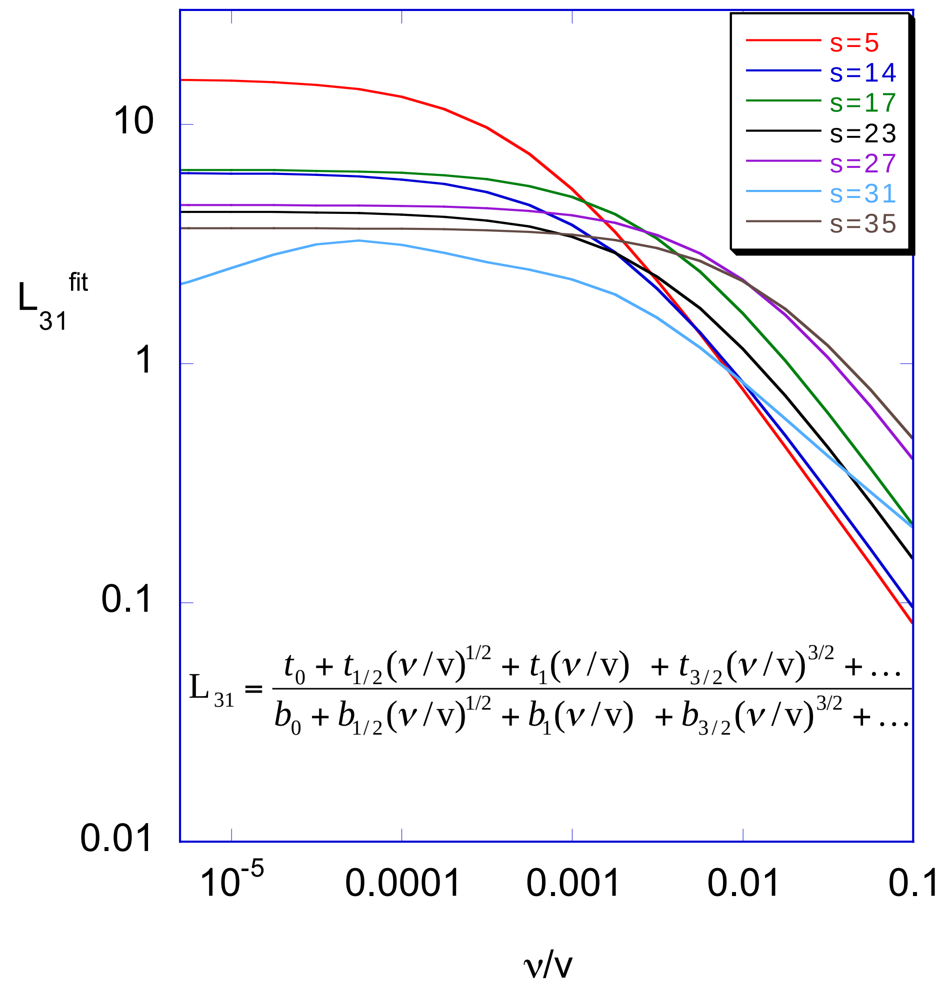

Comparison of DKES predicted bootstrap current profiles with collisionless limit

- Collisionless limit based on BOOTSJ code of L. Berry/J. Tolliver - includes damping to avoid singularities at rational surfaces
- Based on:
  - K.C. Shaing, B.A. Carreras, N. Dominguez, V.E. Lynch, J.S. Tolliver, "Bootstrap current control in stellarators", Phys. Fluids B1, 1663 (1989)
  - K.C. Shaing, E.C. Crume, Jr., J.S. Tolliver, S.P. Hirshman, W.I. van Rij. "Bootstrap current and parallel viscosity in the low collisionality regime in toroidal plasmas", Phys. Fluids B1, 148 (1989).
  - K.C. Shaing, S.P. Hirshman, J.S. Tolliver "Parallel viscosity-driven neoclassical fluxes in the banana regime in nonsymmetrical Toroidal plasmas", Phys. Fluids 29, 2548 (1986).

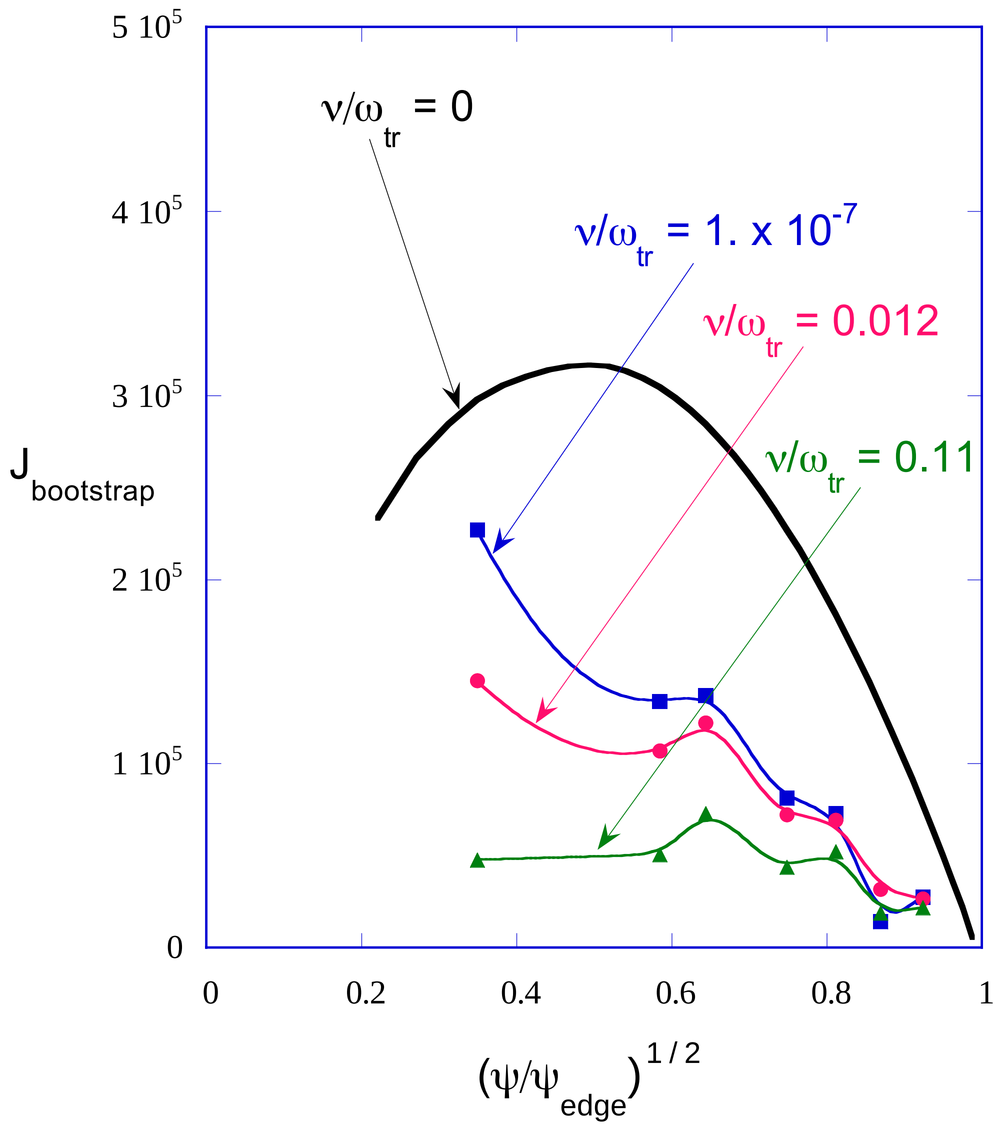

Monte Carlo procedure for estimating global energy lifetimes (DELTA5D code)

DELTA5D Monte Carlo

- start with particles distributed over cross section using PDF's consistent with assumed profiles and local Maxwellians
- follow ensemble in time, replacing particles (consistent with initial PDF's) as they leave outer surface
- Record energies of escaping particles - use to calculate τ_E
- Follow until approximate steady–state is achieved
- Vary potential (with fixed profile shape) to achieve global ambipolar balance of electron/ion particle loss rates

Typical initial Maxwellian particle loading for T = 500eV $(1 - \psi/\psi_{max})^2$

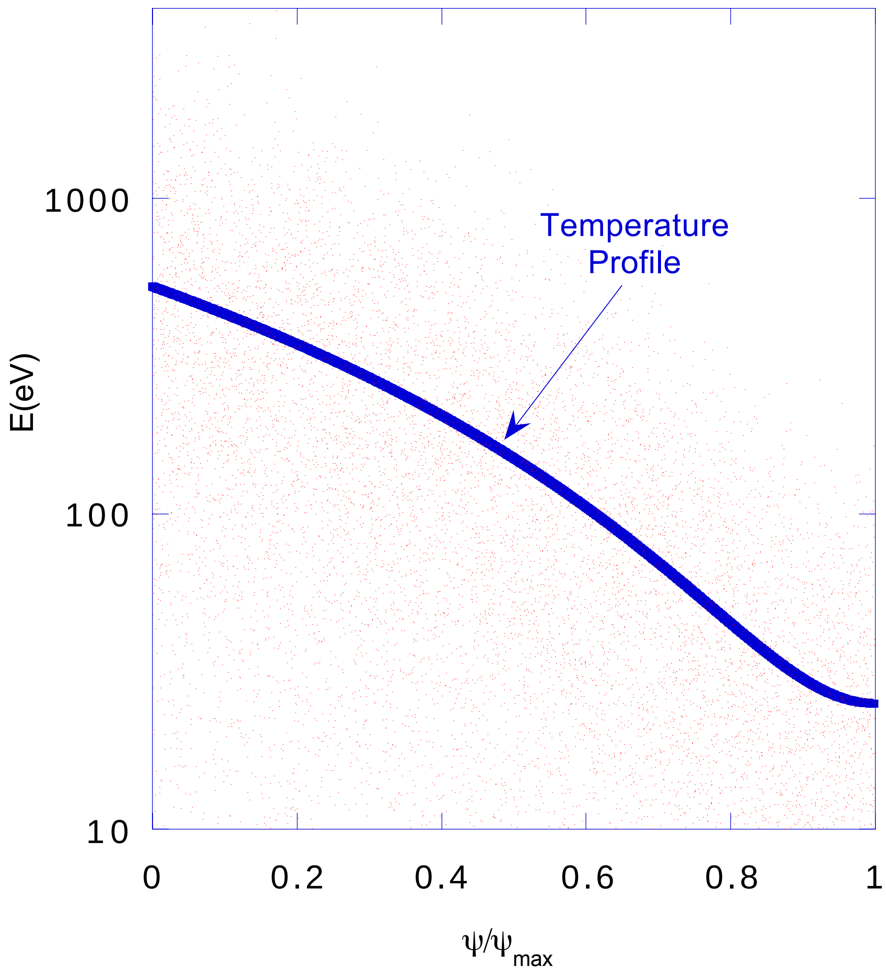

Power flows for global single species test particle simulations:

DELTA5D Monte Carlo

- To achieve steady state, in a reasonable simulation time, terms (1) and (2) need to be balanced:
- For $E_r = 0$
  - can include pitch angle and energy scattering if $Q_{ii} + Q_{ei}$ is weak during particle confinement time
  - or can include only pitch angle scattering
- For $E_r \neq 0$
  - rely on $Q_{ii} + Q_{ei}$ term (1) to redistribute energy loss/gain from term (2)
  - or can remove kinetic energy loss/gain (due to $e\Delta\phi$) each time step

$$\frac{dW_{test,ion}}{dt} = \int \left(Q_{ii} + Q_{ei}\right) d^3v \qquad (+/-) \quad (1)$$

$$+ \int \vec{J} \bullet \vec{E}\ d^3v \qquad (+/-) \quad (2)$$

$$(-) \quad (3)$$

$$+ \int \frac{dW_{surface-loss}}{dt} dS \qquad (+/-) \quad (4)$$

$$+ \int N_{replacement} \left[T(\psi) + e\phi\right] d^3v$$

$$\frac{dW_{test,electron}}{dt} = \quad Similar \ \ equations$$

Monte Carlo studies of global ion confinement times for ICH parameters between devices (all at same R_0) and for different coil currents

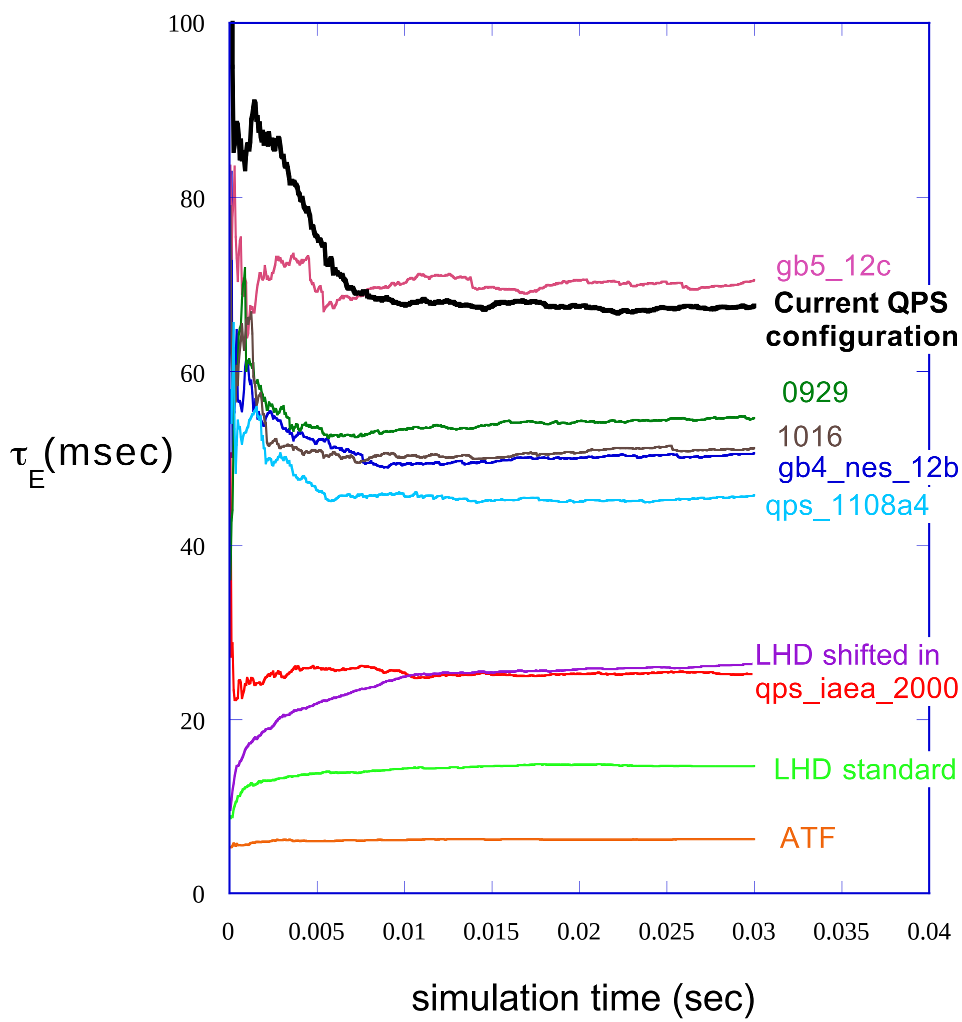

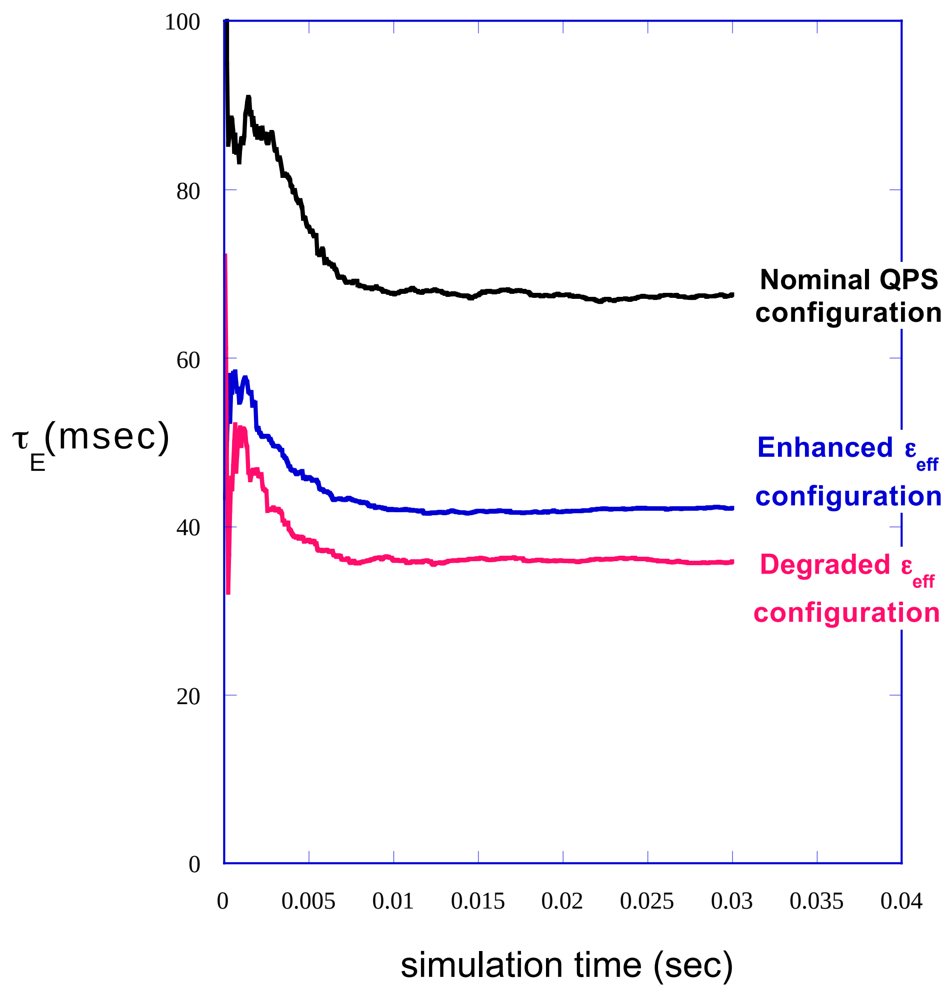

Monte Carlo studies of global ion confinement times for ECH parameters between devices (all at same R_0) and in QPS for different coil currents

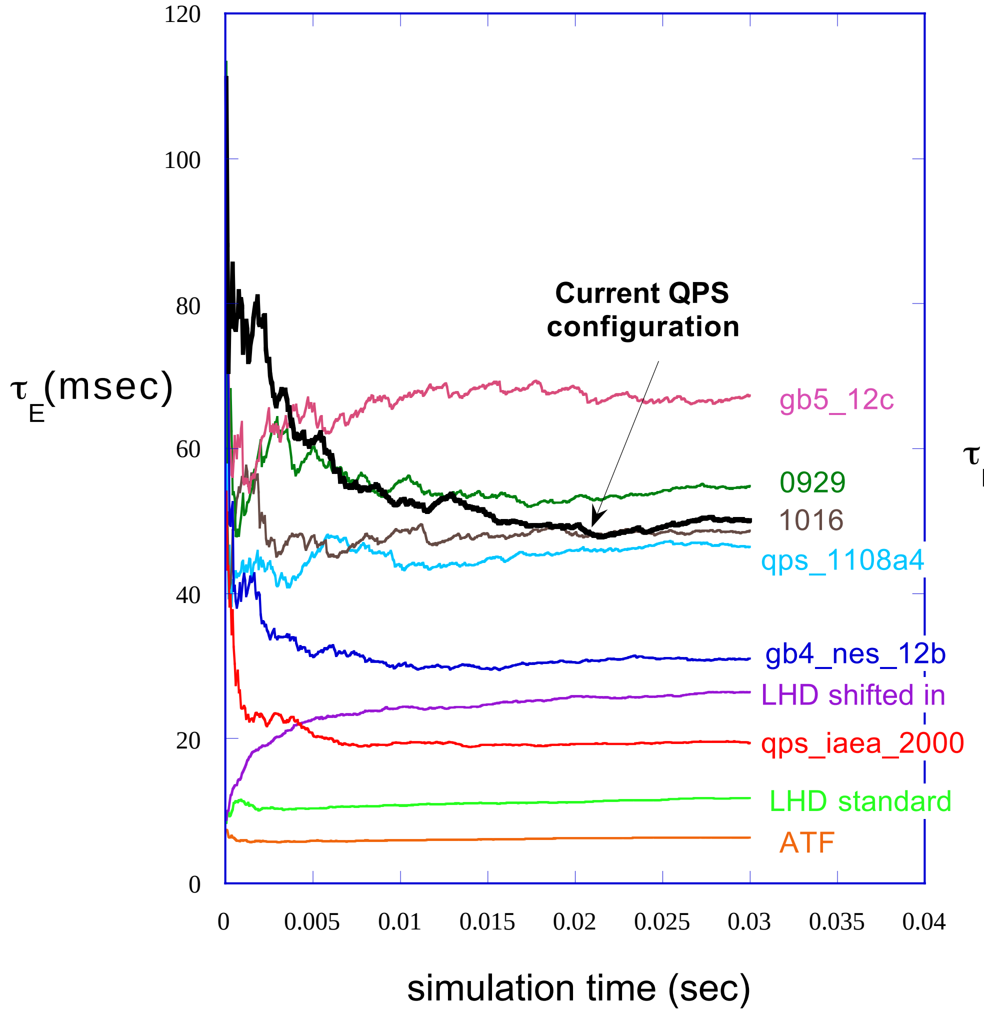

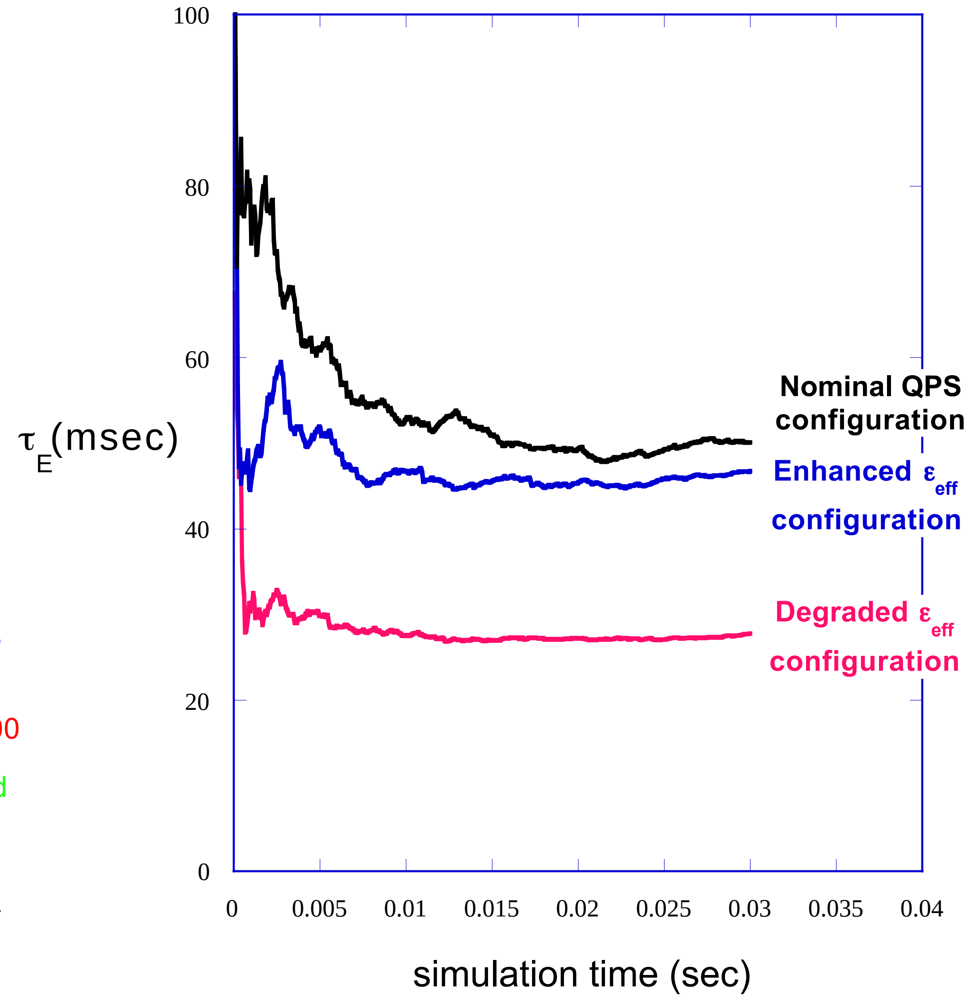

δf Bootstrap Current Calculation

[uses method of A. Boozer and M. Sasinowski, Phys. Plasmas **2** (1995) 610]

$$f = f_M + \delta f \qquad f_M = \frac{n}{(2\pi kT)^{3/2}} e^{-mv^2/kT}$$

$$\frac{d(\delta f)}{dt} - C(\delta f) = -\frac{\partial \psi}{\partial t}\frac{\partial f_M}{\partial \psi}$$

$$\delta f = -(\psi - \psi_0)\frac{\partial f_M}{\partial \psi}$$

(evaluated at particle locations)

$$J_{bootstrap} = q\int d^3x \;\; d^3\mathrm{v}\; \mathrm{v}_{\|}\delta f$$

$$= \frac{2\pi q}{\int d^3x \;\; g^{-1/2}}\int \mathrm{v}^2 d\mathrm{v} \;\; d\lambda \;\; d^3x \;\; \mathrm{v}_{\|} \;\; g^{-1/2} \;\; \delta f$$

with $\sqrt{g} = \text{Jacobian} = \mu_0(G + \iota I)/B^2$

$$J_{bootstrap} = -4\pi\int \mathrm{v}^2 d\mathrm{v}\; \mathrm{K}(\psi,\,\mathrm{v},\,\mathrm{t})\frac{\partial f_M}{\partial \psi}$$

where $K(\psi,\,\mathrm{v},\,\mathrm{t}) = \dfrac{\sum_{\mathrm{i}=1}^{\mathrm{N}} \mathrm{v}_{\|,\mathrm{i}}(\psi_i - \psi_0) g_i^{-1/2}}{2\sum_{\mathrm{i}=1}^{\mathrm{N}} g_i^{-1/2}}$

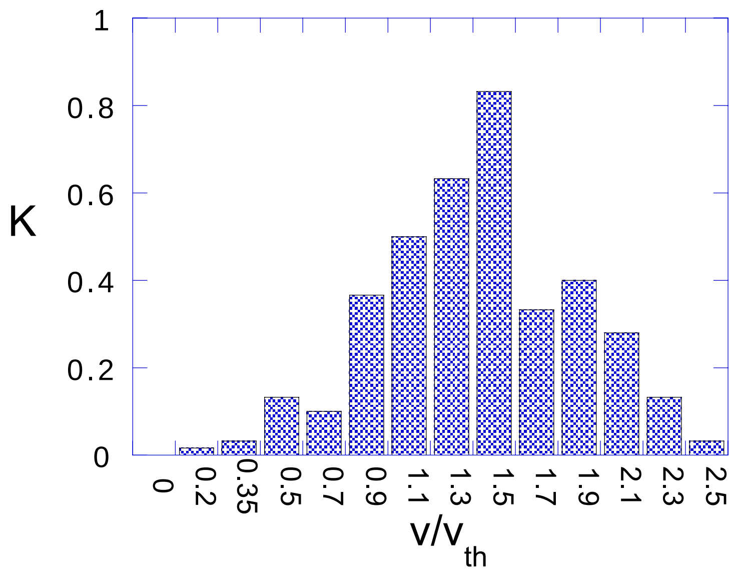

δf Monte Carlo scan of Bootstrap current vs. flux surface

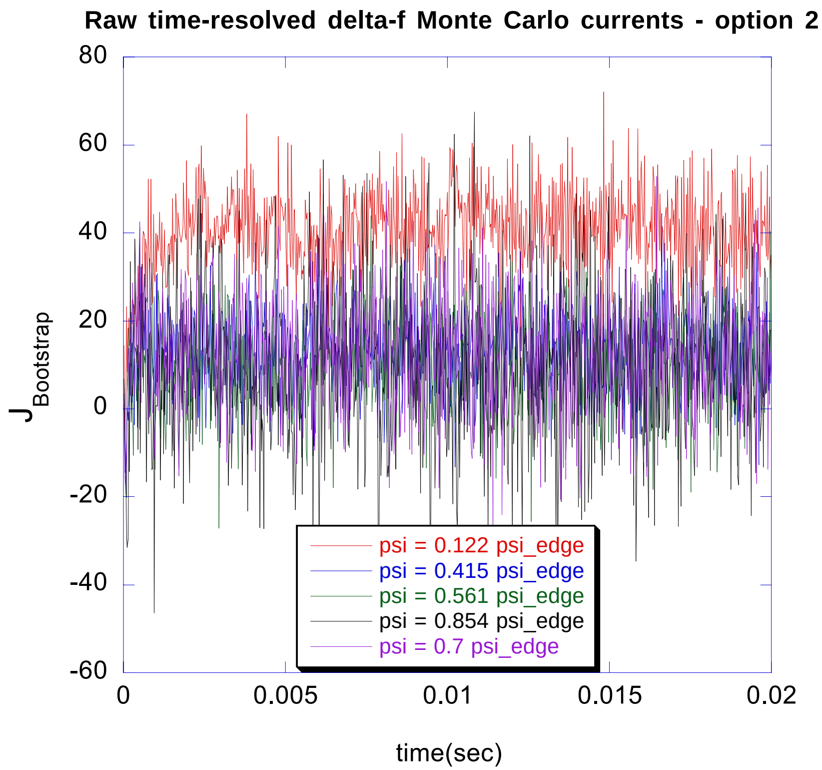

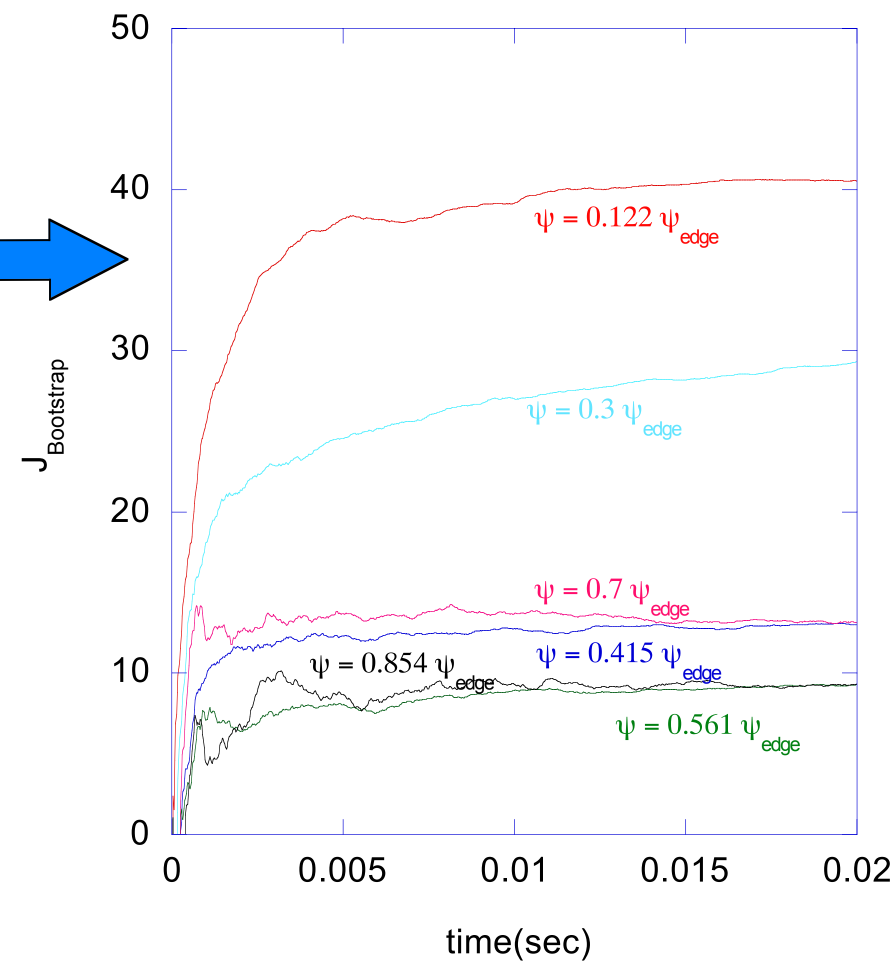

δf Monte Carlo Bootstrap current: profile and error bars

(Error bars are based on one standard deviation away from the mean in the above saturated time resolved currents)

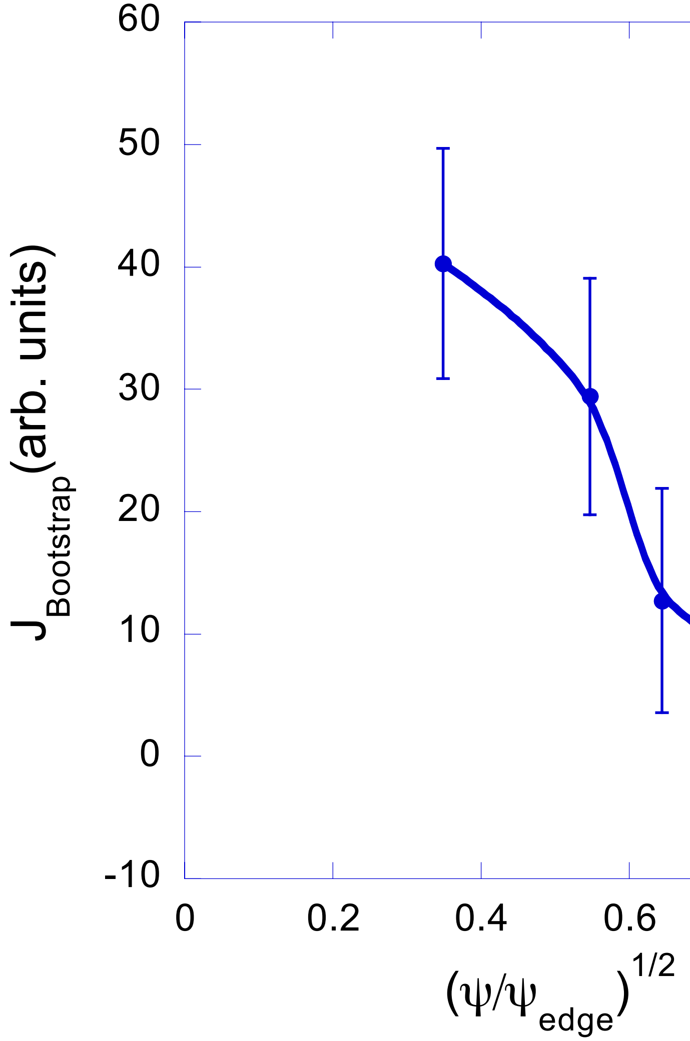

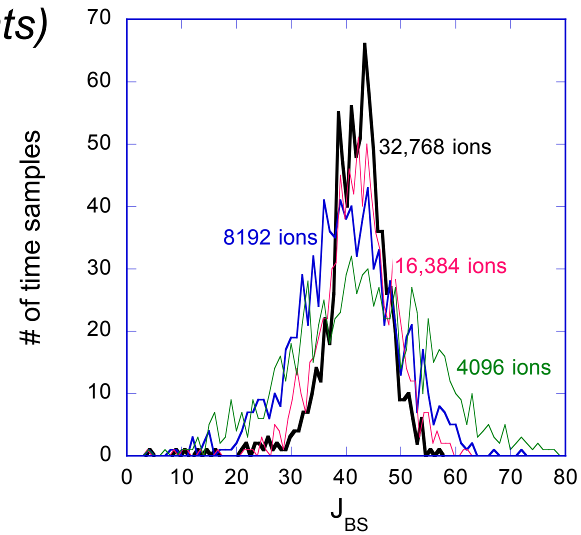

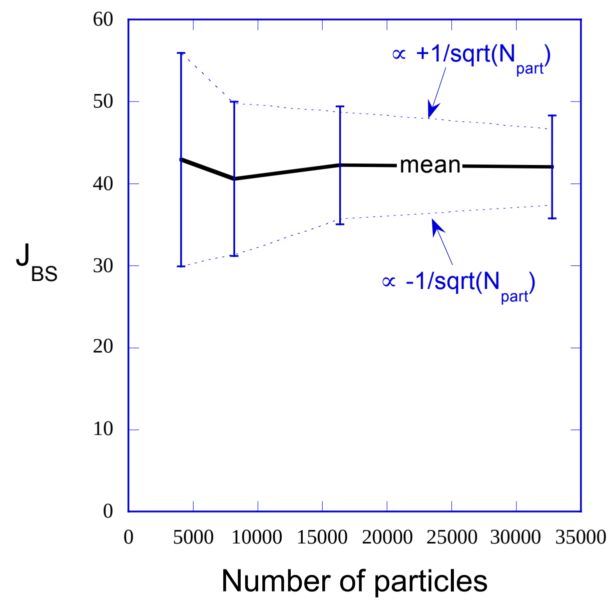

High β configuration: |B| contours start to close and align with ψ:

β=0%

β=23%

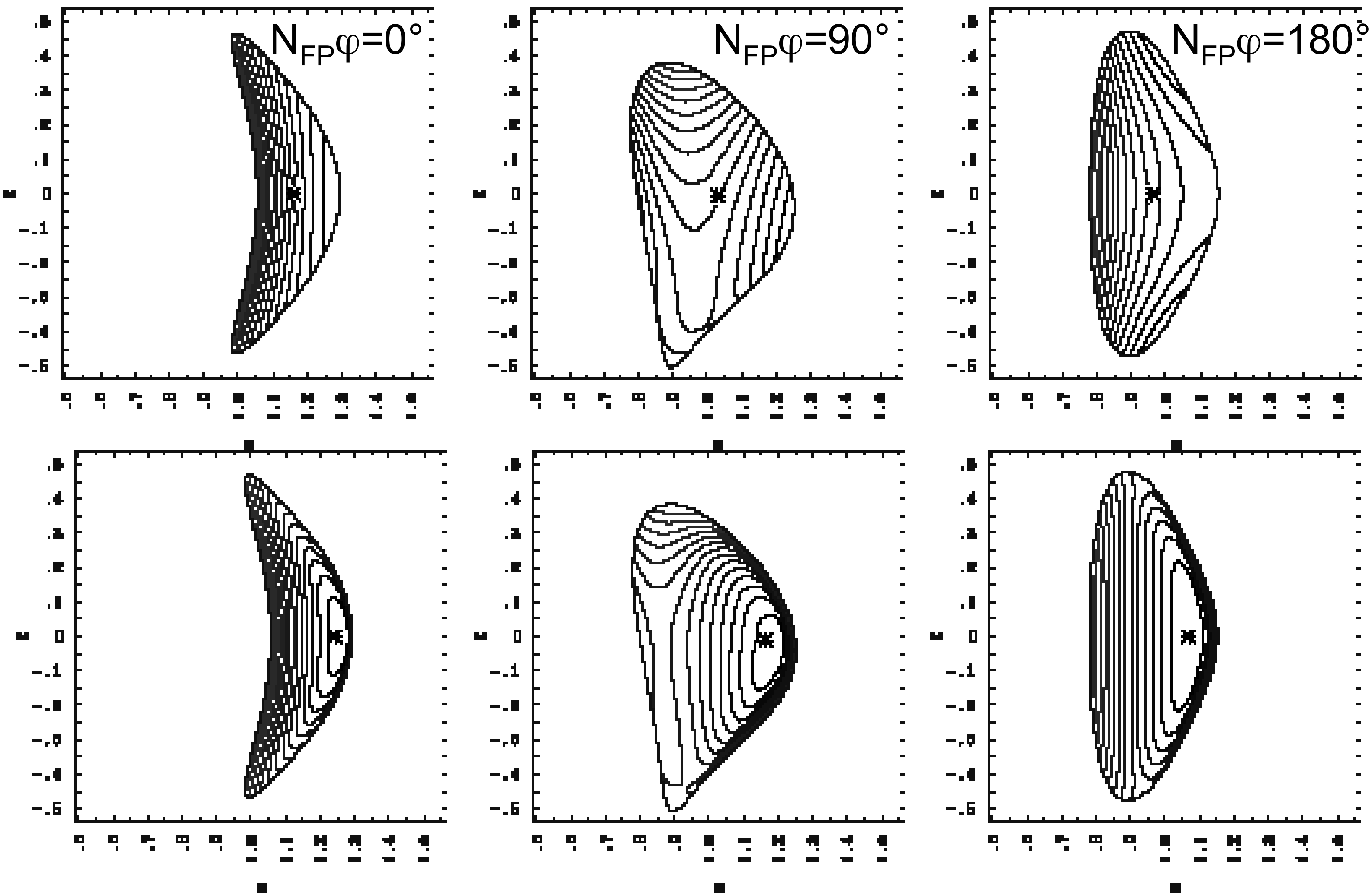

α-particle slowing-down simulations show these devices indicate very good confinement with increasing β.

Alpha confinement

The configuration was scaled to <B> = 5T and R_0 = 10m for alpha confinement studies

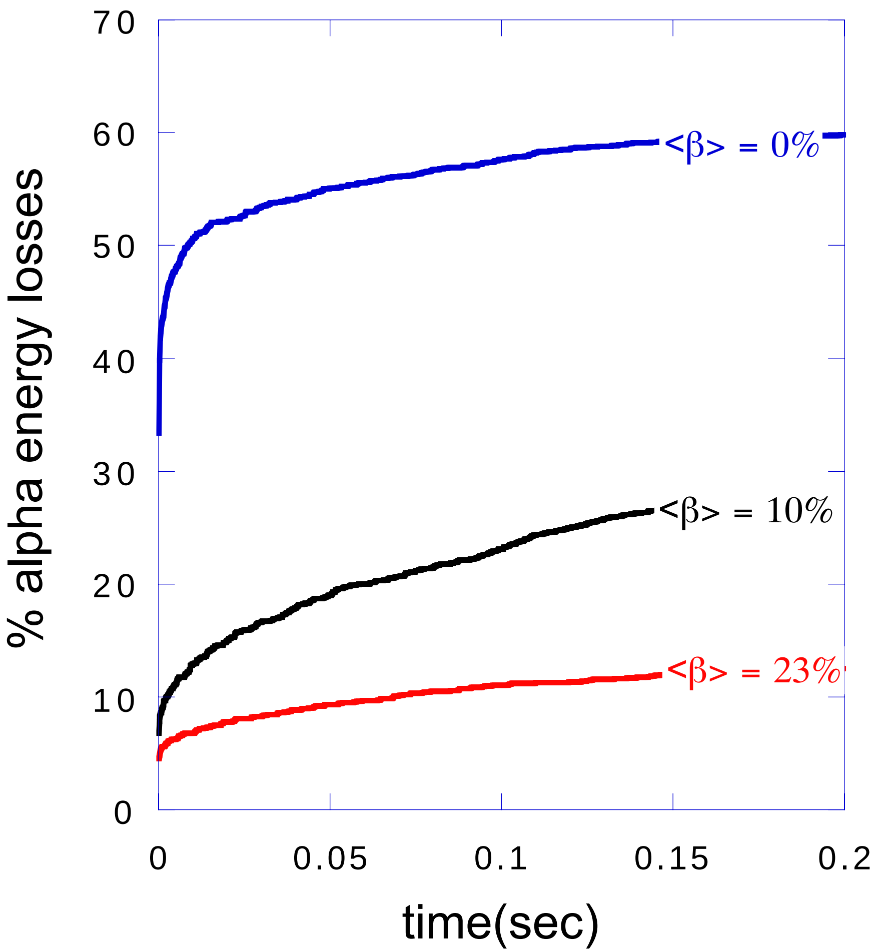

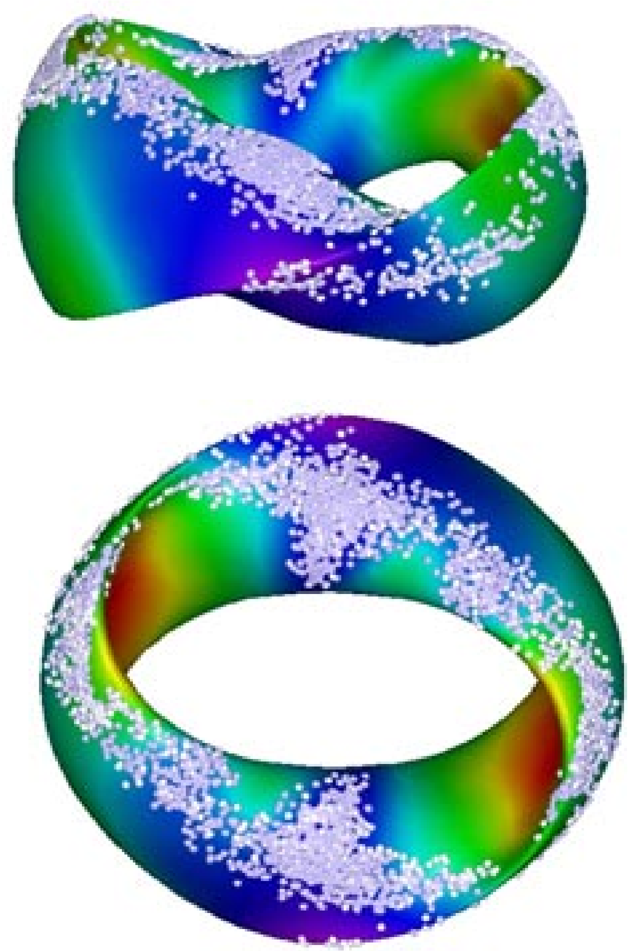

Fast ion driven Alfvén Instabilities

- Motivations for study of stellarators Alfvén instabilities
  - Seen experimentally (W7-AS, CHS, LHD)
    - A. Weller, D. A. Spong, et al., Phys. Rev. Lett. **72**, 1220 (1994); K. Toi, et al., Nucl. Fusion **40**, 149 (2000); A. Weller, et al., Phys. of Plasmas **8** 931(2001)
  - Enhanced loss of fast ions
  - Diagnostic use (MHD spectroscopy)
  - Channeling of fast ion energy to thermal ions
- Low aspect ratio configurations provide a new environment for Alfvén studies
  - Stronger equilibrium mode couplings
  - Lower number of field periods lead to
    - More closely coupled toroidal modes (n_0, $\pm\, n_0 \pm N_{fp}$, etc.)
    - This leads to HAE (Helical Alfvén) couplings at lower frequencies

Alfvén Gap structure using STELLGAP code

Stellarator Alfvén Couplings

Alfvén coupling condition: $k_{\|,m,n} = -k_{\|,(m+\Delta),(n+\alpha N_{fp})}$

$\Delta,\ \alpha = \text{integers}$

$$n - m\iota = -\left(n + \alpha N_{fp} - m\iota - \Delta\iota\right)$$

$$\iota = \frac{2n + \alpha N_{fp}}{2m + \Delta} \qquad \omega = \frac{v_A}{R}\frac{\Delta n - \alpha m N_{fp}}{2m + \Delta}$$

- GAE (global Alfvén mode): $\alpha = 0,\ \Delta = 0$
- TAE (toroidal Alfvén mode): $\alpha = 0,\ \Delta = \pm 1$
- EAE (elliptical Alfvén mode): $\alpha = 0,\ \Delta = \pm 2$
- NAE (noncircular Alfvén mode): $\alpha = 0,\ |\Delta| > 2$
- MAE (mirror Alfvén mode): $\alpha = 1,\ \Delta = 0$
- HAE (helical Alfvén mode): $\alpha = 1,\ \Delta \neq 0$

This leads to a set of 3 coupled equations. A singularity condition gives the Alfvén continuum

[A. Salat, J. A. Tataronis, Phys. Plasmas 8, 1200 (2001)]

$$\begin{cases} L^{11}V = \dfrac{|B|^2}{G+\iota I}\left[I\dfrac{\partial W_1}{\partial \zeta} - G\dfrac{\partial W_1}{\partial \theta}\right] - L^{21}W_2 + \dfrac{\left(\vec{J}\cdot\vec{B}\right)}{G+\iota I}\left(\iota\dfrac{\partial W_2}{\partial \theta} + \dfrac{\partial W_2}{\partial \zeta}\right) \\[2ex] \dfrac{\partial W_1}{\partial \psi} = \dfrac{1}{|B|^2}\left(L^{22}W_2 + L^{21}V\right) + \dfrac{\left(\vec{J}\cdot\vec{B}\right)}{G+\iota I}\left(\iota\dfrac{\partial V}{\partial \theta} + \dfrac{\partial V}{\partial \zeta}\right) \\[2ex] \dfrac{\partial W_2}{\partial \psi} = -|B|^2 W_1 + \dfrac{1}{G+\iota I}\left(G\dfrac{\partial V}{\partial \theta} - I\dfrac{\partial V}{\partial \zeta}\right) \end{cases}$$

$$V = E_1$$
$$W_1 = i\omega B_3$$
$$W_2 = E_2$$
$$with \quad r^1 = \psi$$
$$r^2 = \theta - \iota\zeta$$
$$r^3 = I(\psi)\theta - G(\psi)\zeta$$
$$\iota = rotational \;\; transform$$
$$G = poloidal \;\; current$$
$$I = toroidal \;\; current$$

$$where \quad L^{11} = \mu_0\rho\omega^2\frac{g^{\psi\psi}}{|B|^2} + \vec{B}\bullet\vec{\nabla}\frac{g^{\psi\psi}}{|B|^2}\vec{B}\bullet\vec{\nabla}$$

$$L^{21} = \mu_0\rho\omega^2\frac{\left(g^{\theta\psi} - \iota g^{\zeta\psi}\right)}{|B|^2} + \vec{B}\bullet\vec{\nabla}\frac{\left(g^{\theta\psi} - \iota g^{\zeta\psi}\right)}{|B|^2}\vec{B}\bullet\vec{\nabla}$$

$$L^{21} = \mu_0\rho\omega^2\frac{\left(g^{\theta\theta} - 2\iota g^{\zeta\theta} + \iota^2 g^{\zeta\zeta}\right)}{|B|^2} + \vec{B}\bullet\vec{\nabla}\frac{\left(g^{\theta\theta} - 2\iota g^{\zeta\theta} + \iota^2 g^{\zeta\zeta}\right)}{|B|^2}\vec{B}\bullet\vec{\nabla}$$

Singular for Alfvén continuum condition : $L^{11}V = 0$

Stellarator Alfvén Continuum Equation

The continuum equation in general geometry (low β) can be written:

$$\mu_0 \rho \omega^2 \frac{|\nabla\psi|^2}{B^2} E_\psi + \vec{B}\cdot\vec{\nabla}\left\{\frac{|\nabla\psi|^2}{B^2}(\vec{B}\cdot\vec{\nabla})E_\psi\right\} = 0 \qquad (1)$$

This can be written in Boozer coordinates using the following:

$$\vec{B}\cdot\vec{\nabla} = \frac{1}{\sqrt{g}}\left(\iota\frac{\partial}{\partial\theta} + \frac{\partial}{\partial\zeta}\right) \quad \text{and} \quad \left|\vec{\nabla}\psi\right|^2 = g^{\rho\rho}\left(\frac{d\psi}{d\rho}\right)^2$$

For devices with stellarator symmetry, the surface displacement can be expanded as follows:

$$E_\psi = \sum_{j=1}^{L} E_\psi^j e_j \quad \text{where} \quad e_j = \cos(n_j\zeta - m_j\theta)$$

Multiplying equation (1) by the Jacobian and integrating over a flux surface then leads to:

$$\mu_0\omega^2\rho\left\langle e_i\sqrt{g}\,\frac{g^{\rho\rho}}{B^2}\sum_{j=1}^{L}E_\psi^j e_j\right\rangle + \left\langle e_i\left(\iota\frac{\partial}{\partial\theta}+\frac{\partial}{\partial\zeta}\right)\frac{g^{\rho\rho}}{B^2\sqrt{g}}\left(\iota\frac{\partial}{\partial\theta}+\frac{\partial}{\partial\zeta}\right)\sum_{j=1}^{L}E_\psi^j e_j\right\rangle = 0$$

Stellarator Alfvén Continuum Equation (contd.)

Integrating by parts then leads to the following symmetric matrix eigenvalue problem:

$$\omega^2 \mathbf{Ax} = \mathbf{Bx}$$

$$where \quad \mathbf{A} = \left[a_{ij}\right] = \mu_0 \rho \left\langle e_i \sqrt{g}\, \frac{g^{\rho\rho}}{B^2} e_j \right\rangle$$

$$\mathbf{B} = \left[b_{ij}\right] = \left\langle \frac{g^{\rho\rho}}{B^2 \sqrt{g}} \left(\iota\!\!\!- \frac{\partial e_i}{\partial \theta} + \frac{\partial e_i}{\partial \zeta} \right) \left(\iota\!\!\!- \frac{\partial e_j}{\partial \theta} + \frac{\partial e_j}{\partial \zeta} \right) \right\rangle$$

$$\mathbf{x} = \left[\xi_s^1 \;\; \xi_s^2 \cdots \xi_s^L \right]^T$$

W7-AS: discharge 40173

[Similar to cases analyzed in A. Weller, D. A. Spong, et al., Phys. Rev. Lett. **72** (1994) 1220]

- In experiment, fluctuations were observed at ~18 kHz
- GAE mode: below the lowest n = 1 continuum
- Such modes can be approximated by cylindrical or axisymmetric models

Continua based on 3d stellarator equilibruim

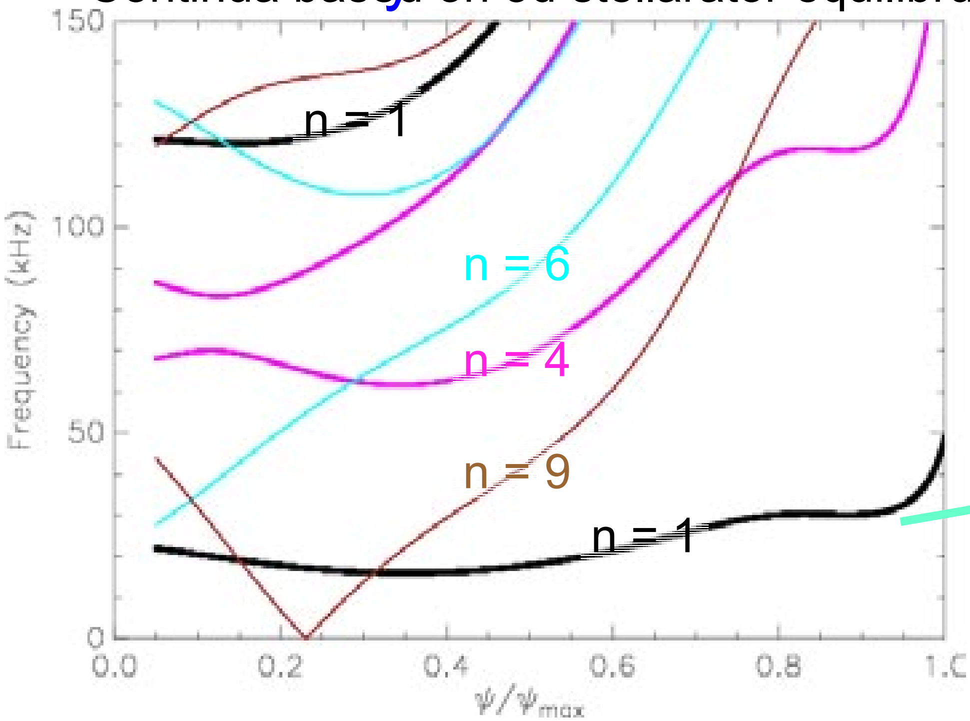

n = 1 GAE continua

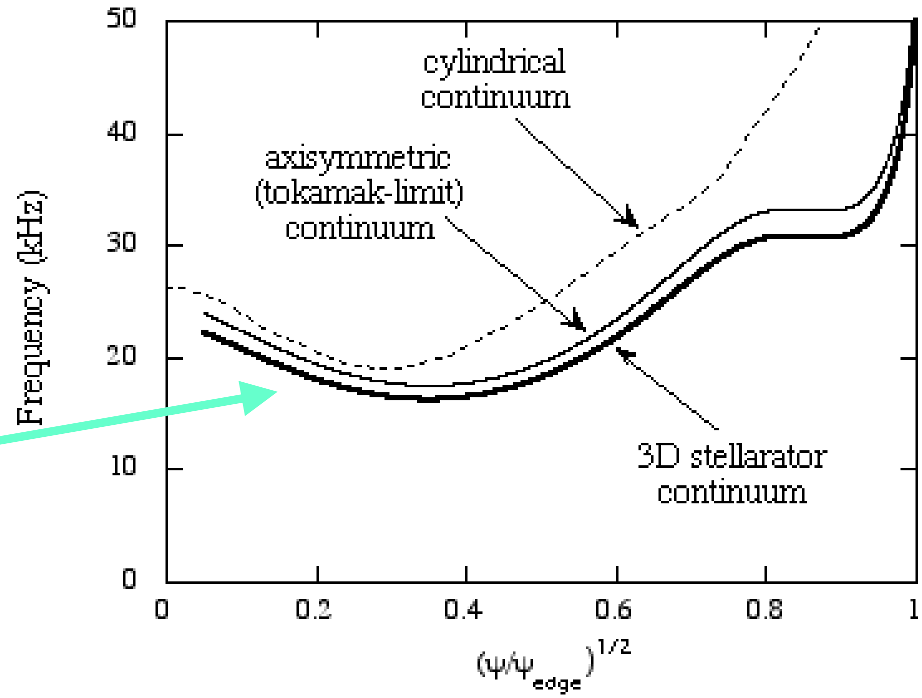

W7-AS: discharge 42873

5 field periods R/<a> = 12

fluctuations observed at 30-50 kHz

Axisymmetric limit

dominant **poloidal** mode is color coded

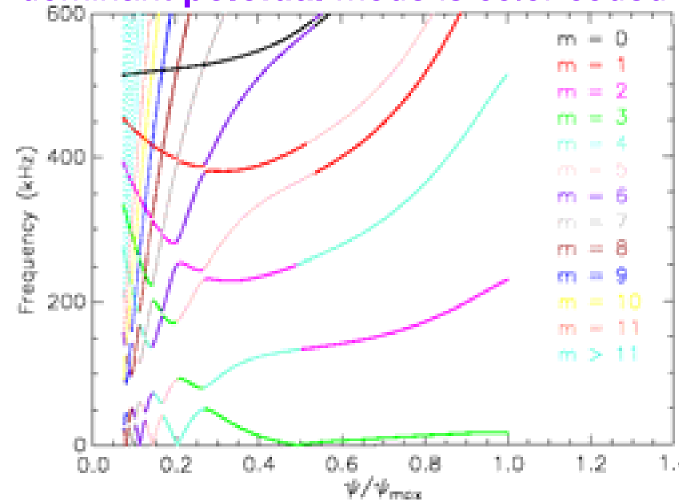

Continua with multiple toroidal modes

n = 1 mode family stellarator continua

dominant **toroidal** mode is color coded

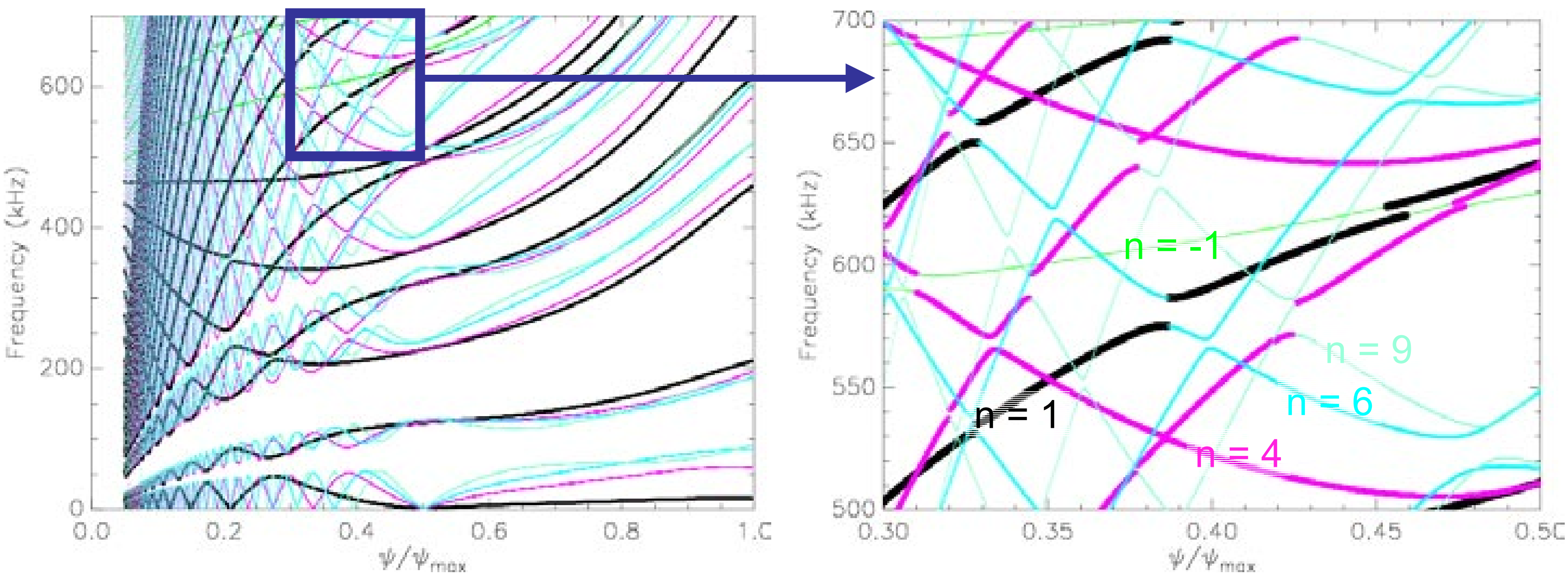

W7-AS: discharge 43348

fluctuations observed at: 30-40, 50-60, 85-100, 125-150, 180-200, and 210-240 kHz

Axisymmetric limit
dominant **poloidal** mode is color coded

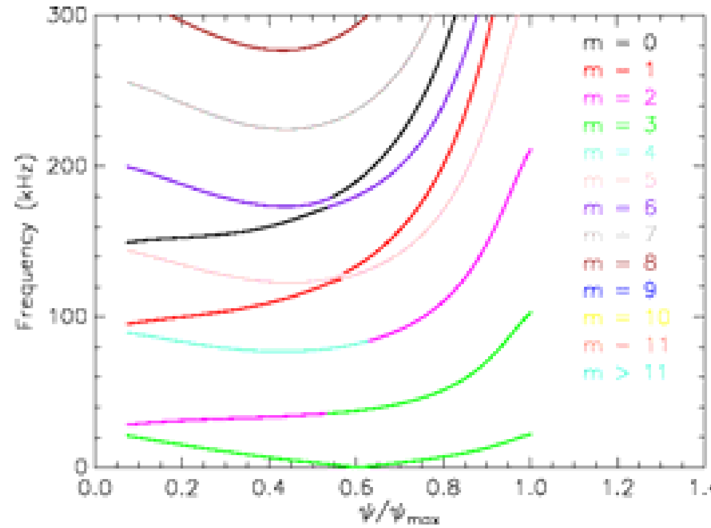

Continua with multiple toroidal modes
n = 1 mode family stellarator continua
dominant **toroidal** mode is color coded

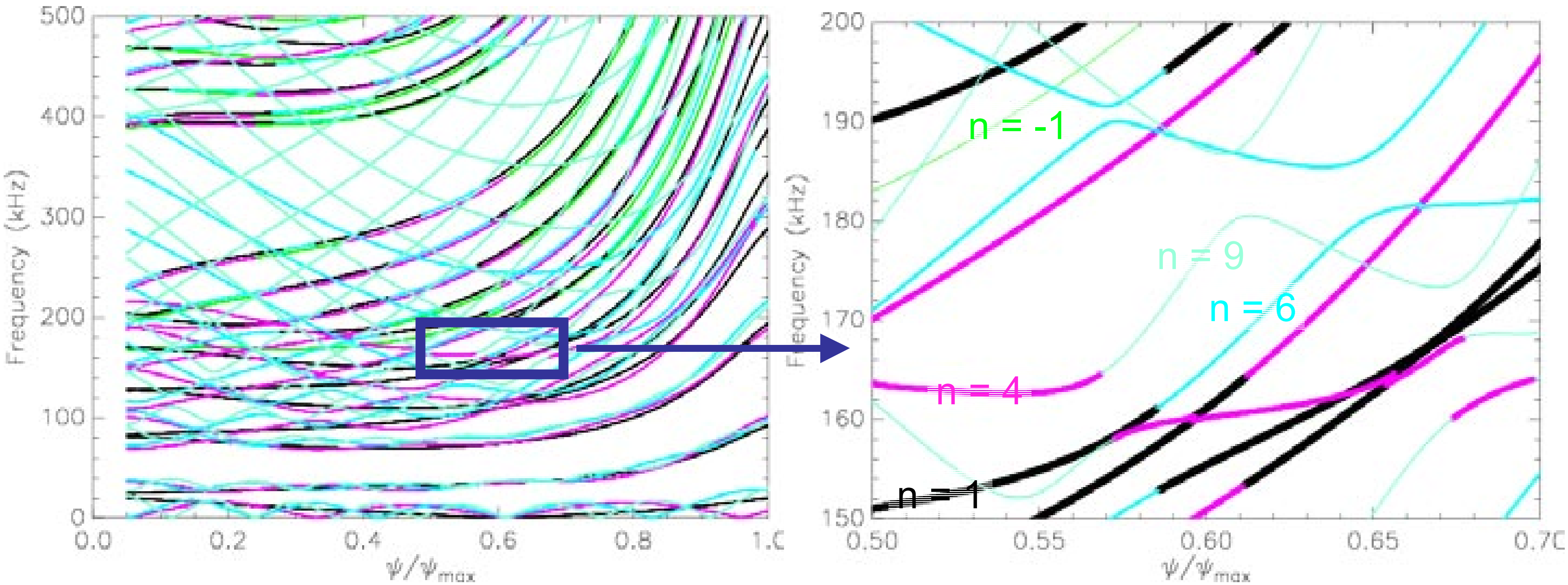

LHD
(10 field periods, R/<a> = 6, torsatron)

Axisymmetric limit
dominant **poloidal** mode is color coded

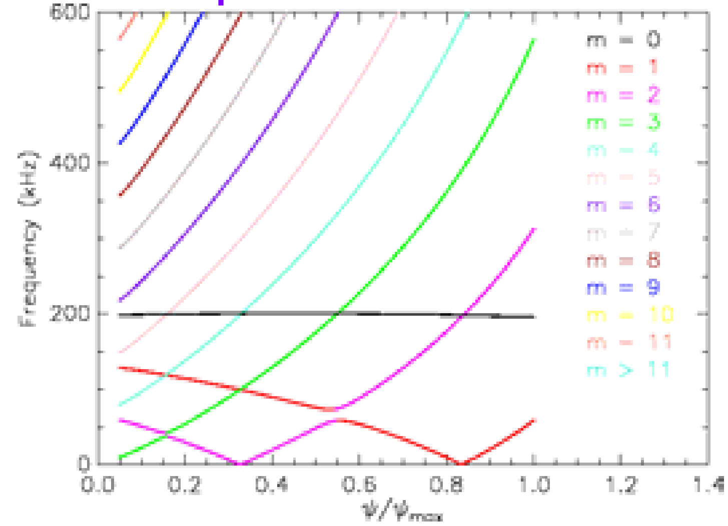

Continua with multiple toroidal modes

n = 1 mode family stellarator continua
dominant **toroidal** mode is color coded

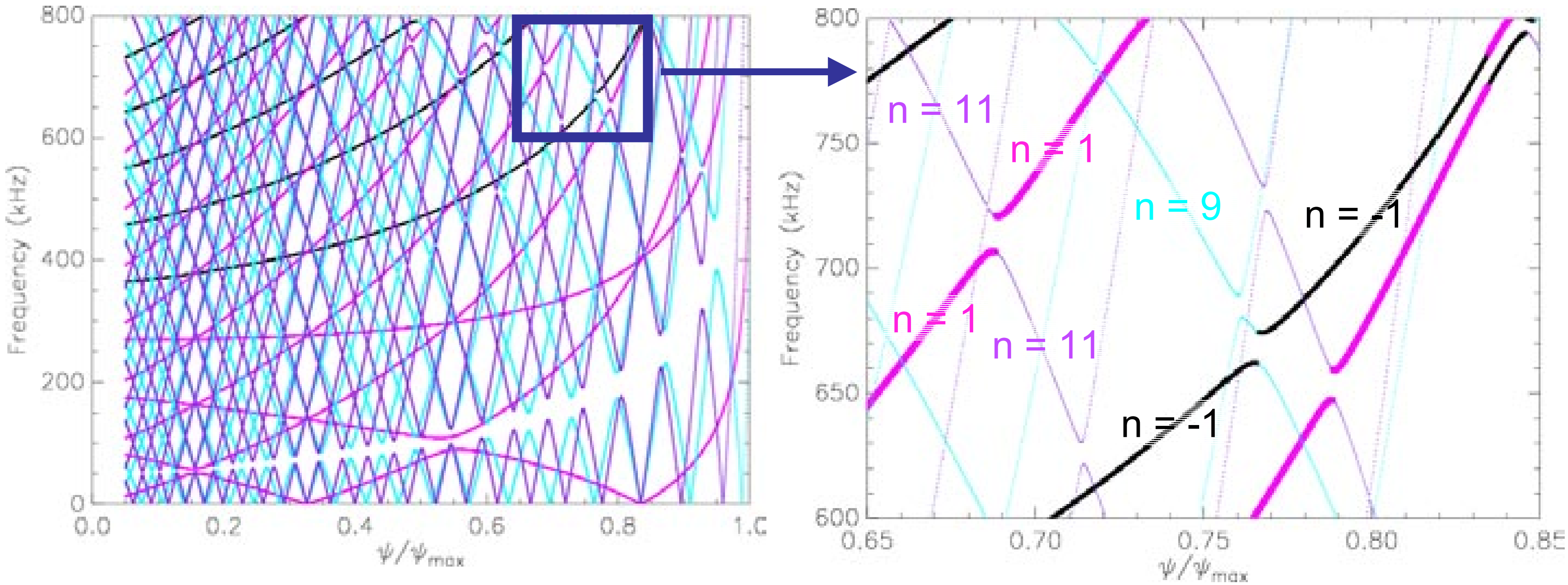

NCSX

3 field period, R/<a> = 4.4
quas-toroidal symmetry

Axisymmetric limit
dominant **poloidal** mode is color coded

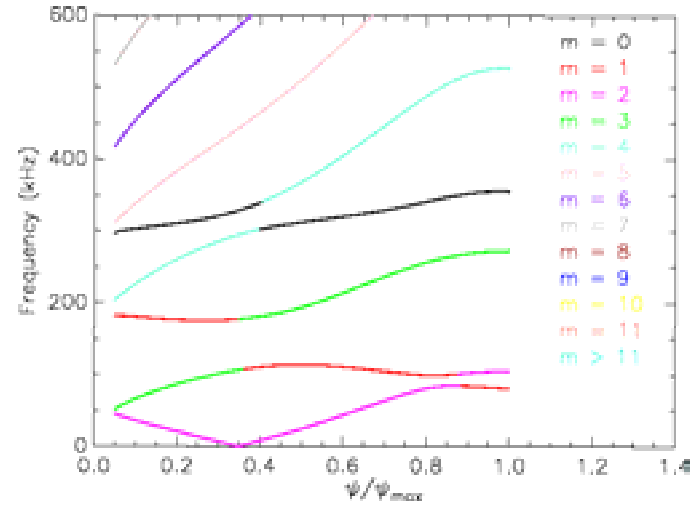

Continua with multiple toroidal modes
n = 1 mode family stellarator continua
dominant **toroidal** mode is color coded

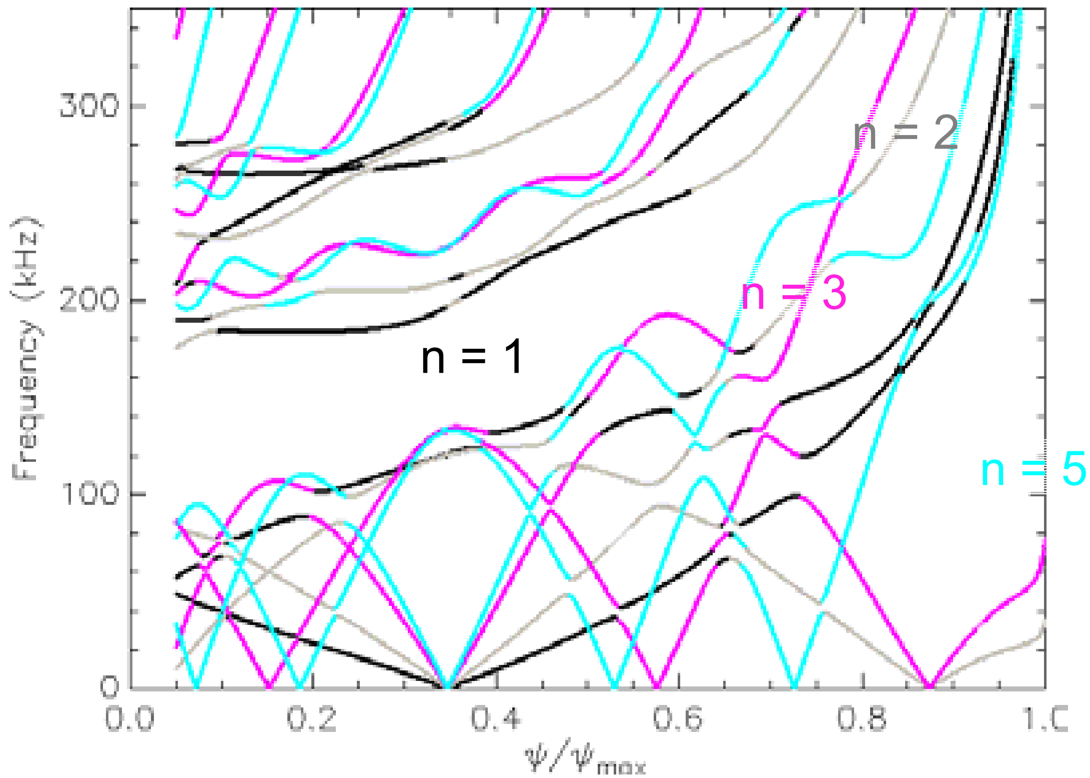

QPS (2 field periods, R/<a> = 2.7, quasi-poloidal symmetry)

n = 1 mode family stellarator continua

dominant **toroidal** mode is color coded

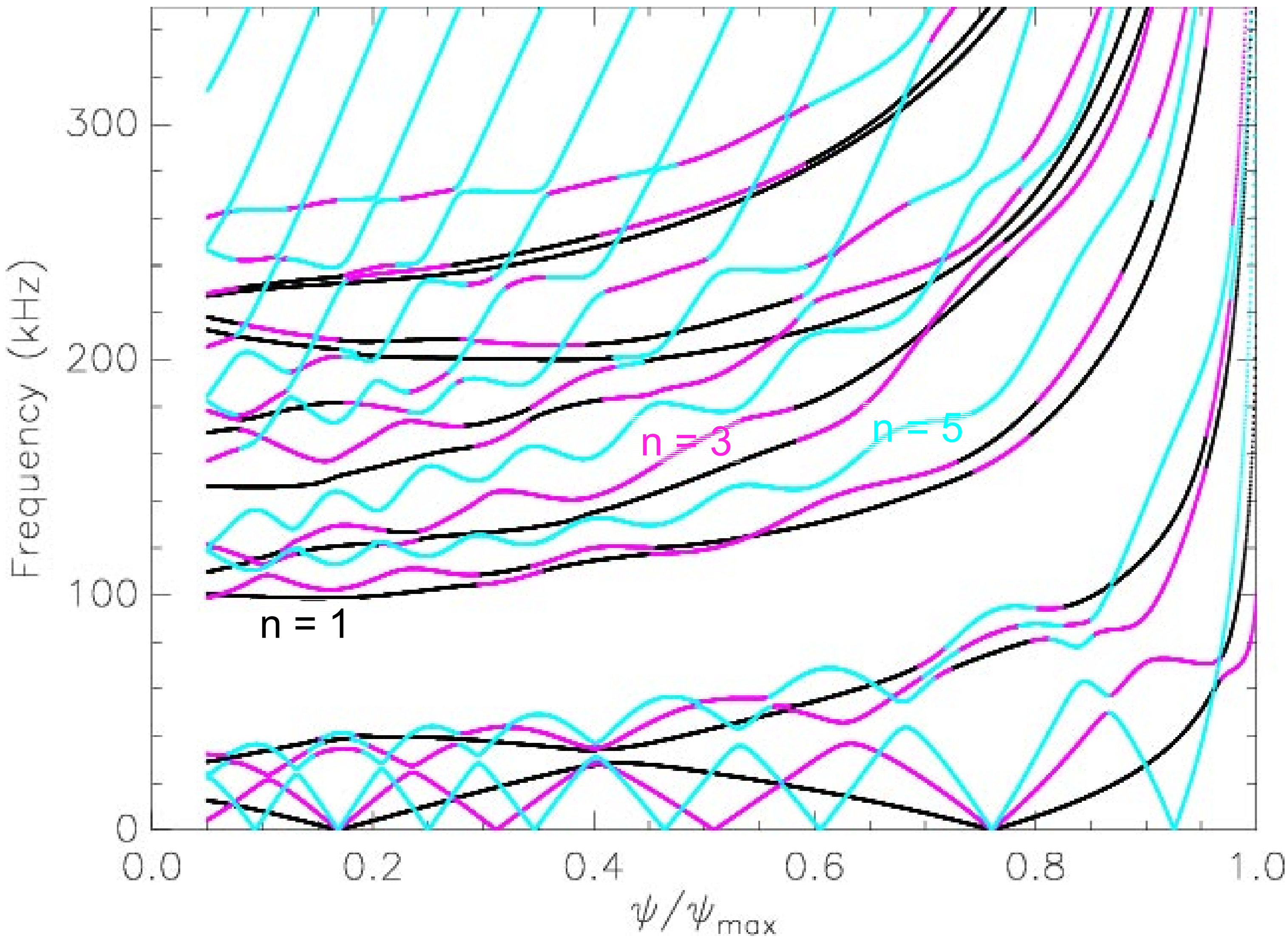

Recently the STELLGAP code has been upgraded to solve the 3 coupled equations for the stable Alfvén mode structure in compact 3D configurations

Discrete 3D Alfvén frequency spectrum (blue = damped red = neutrally stable)

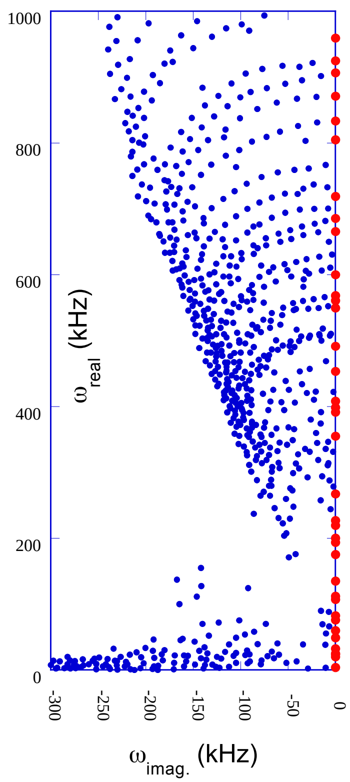

Alfvén Continuum for QA-symmetric stellarator (color indicates dominant toroidal mode number)

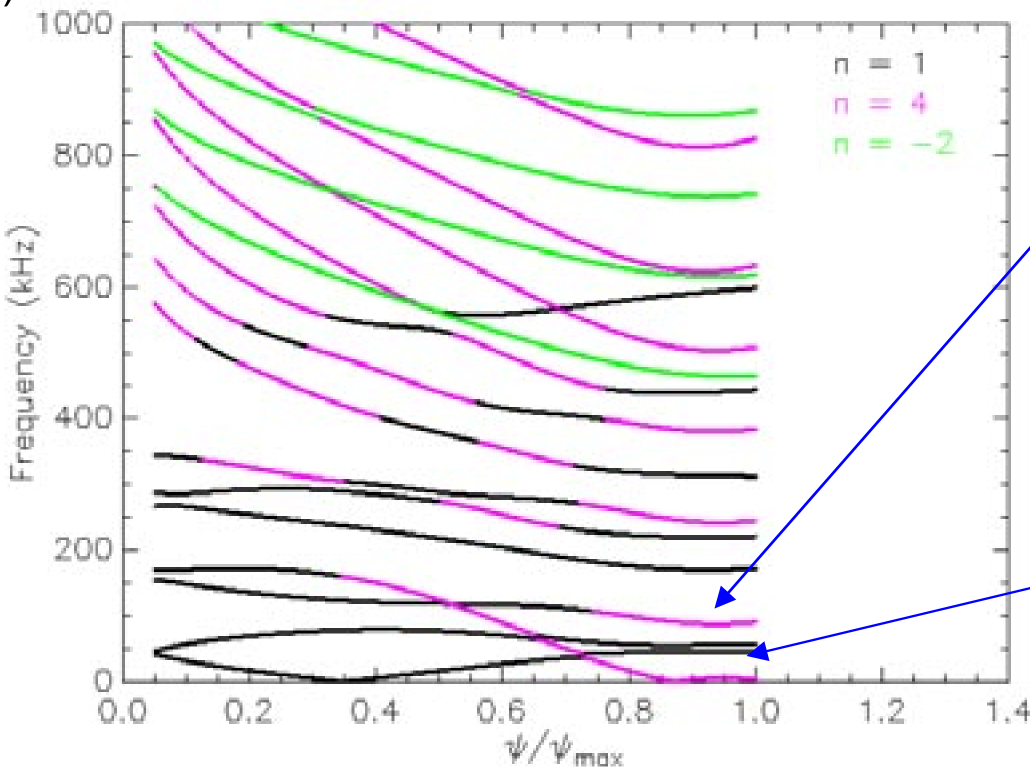

AE radial mode Structure (multiple toroidal modes)

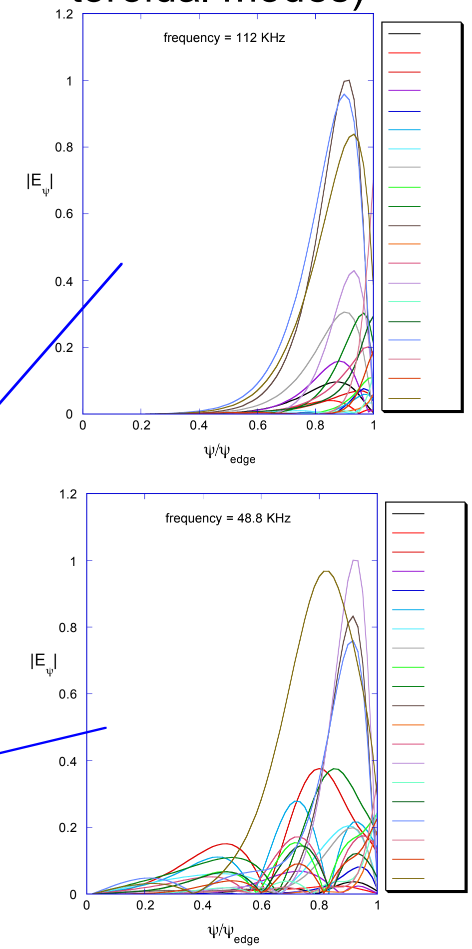

Conclusions

- QPS optimized design provides good confinement at very low aspect ratio
- New physics areas to be tested:
  - Equilibrium robustness for compact geometry
  - Improved neoclassical transport
  - Anomalous transport at low A regime
  - Lowered poloidal flow damping
  - Beta limits
- Substantial flexibility from varying modular coil currents
  - Factor of 50 variation in low collisionality transport
- Good energetic particle confinement at high β
  - Self-induced isodynamic configuration
- STELLGAP code developed for stellarator Alfvén continua and discrete eigenmodes